FACULTY OF ENGINEERING AND ARCHITECTURE

Dynamic Stability Analysis of a Hydrofoiling Sailing Boat using CFD

Alec Bagué
Student number: 01406945

Supervisors: Prof. dr. ir. Joris Degroote, Prof. dr. ir. Evert Lataire
Counsellor: Ir. Toon Demeester

Master's dissertation submitted in order to obtain the academic degree of
Master of Science in Electromechanical Engineering

Academic year 2018-2019

GHENT UNIVERSITY

FACULTY OF ENGINEERING AND ARCHITECTURE

Dynamic Stability Analysis of a Hydrofoiling Sailing Boat using CFD

Alec Bagué
Student number: 01406945

Supervisors: Prof. dr. ir. Joris Degroote, Prof. dr. ir. Evert Lataire
Counsellor: Ir. Toon Demeester

Master's dissertation submitted in order to obtain the academic degree of
Master of Science in Electromechanical Engineering

Academic year 2018-2019

GHENT UNIVERSITY

Acknowledgments

I would like to express my gratitude to prof. Degroote and late prof. Vierendeels who initially set everything into motion for me to propose my own thesis subject. Sailing has always been passion of mine and the opportunity to combine my engineering skills with my sailing experience was very exciting. I would also like to thank prof. Degroote and prof. Lataire for their wise input on the matter and to steer me in the right direction when necessary. Their combined knowledge of CFD, stability dynamics and maritime engineering helped me shape this text. A sincere thank you goes out to ir. Demeester, my counselor, who always responded to my every question. And lastly B. Goodall and L. Verbeeck from Goodall Design for providing me with the exciting design and necessary data.

As this thesis is the final aspect of my 5-year engineering education, I would like to thank everyone who helped me along the way: family, friends, professors, staff, ... Thank you!

Permission for usage

Dynamic Stability Analysis of a Hydrofoiling Sailing Boat using CFD

by

Alec Bagué

Supervisors: Prof. dr. ir. Joris Degroote, Prof. dr. ir. Evert Lataire
Counsellor: Toon Demeester

Master's dissertation submitted in order to obtain the academic degree of
Master of Science in Electromechanical Engineering

Department of Flow, Heat and Combustion Mechanics

Faculty of Engineering and Architecture
Ghent University

Academic year 2018-2019

Abstract

This thesis handles the development of a framework on how to perform a dynamic stability analysis for a hydrofoiling boat using CFD and applies this framework to an existing design called the *"Goodall Design Foiling Viper"*. It discusses the dynamic stability analysis of airplanes as the principles of hydrofoil boats and airplanes are similar. From this theory, an adjusted model is proposed specifically for the case at hand. A stability analysis has two distinct parts: calculation of the equilibrium state and calculation of the stability derivatives for the stability matrix. A fluid-structure interaction algorithm was created to calculate the equilibrium state of a hydrofoil boat. To limit simulation time, approximations were proposed for the calculation of the stability derivatives. The application of the framework to the Viper resulted in a stability matrix with 5 eigenmodes: 1 real mode and 2 complex conjugated pairs. The real mode was dominated by coupled motion of the forward velocity and the horizontal position of the bat. Both complex pairs resulted in some kind of wobbling motion: an oscillatory motion of pitch and heave.

Keywords

foiling, dynamic stability analysis, sailing, computational fluid dynamics, fluid-structure interaction

Dynamic Stability Analysis of a Hydrofoiling Sailing Boat using CFD

Alec Bagué

Supervisor(s): Prof. dr. ir. J. Degroote, Prof. dr. ir. E. Lataire, ir. T. Demeester

Abstract—**This paper handles the study on the stability of a hydrofoiling sailing boat called the *"Goodall Design Foiling Viper"*. The goal of *Goodall Design* is to make hydrofoiling accessible to a wider public, whereas it was previously reserved for professional sailors at the highest level of the sport. To allow for safe operation, stability is an essential characteristic of the boat. The goal of this work is to find a strategy on how to perform a dynamic stability analysis using computational fluid dynamics (CFD). This paper starts by establishing a theoretical framework to perform the dynamic stability analysis. This stability analysis is then performed around an equilibrium state which depends on operating parameters such as speed, centre of gravity, ... This work also focuses on an FSI strategy to determine these equilibrium states. The last part discusses the stability characteristics of the Viper.**

Keywords— **foiling, dynamic stability analysis, sailing, computational fluid dynamics, fluid-structure interaction**

Fig. 1. The Goodall Design Foiling Viper hovering above the water.

I. Introduction

THIS paper handles the development of a framework for performing a dynamic stability analysis for a hydrofoiling boat and applies this framework to the "Goodall Design Foiling Viper" (hereafter called Viper). Hydrofoiling is the practice where a normally buoyant vessel is fitted with lifting surfaces below the water surface which generate a vertical force. This lift will then partly or completely replace the buoyant force of the hull. If this force becomes sufficiently large, it will lift the hull out of the water as if the boat would be flying. As the hull is lifted from the water, there is an ensuing reduction of the drag as now only the hull's appendages are submerged. This is a clear advantage as it allows for greater speeds for the same propulsive power. Hydrofoils are one of the major developments of the last decades within the sport of sailing. They were initially introduced at the highest level of the sport, but today there is an urge to make this development accessible to a wider public. The increase in speed and the different way of sailing has however led to new and greater risks, various accidents have already occurred [1]. In the pursuit of making foiling more widely available, safety is one of the primary concerns. One way of providing sufficient safety is to examine and improve the stability of hydrofoil boats as this will lead to more predictable behaviour and easier handling. This is the main motivation for this work.

The Viper is a 16 feet (5 meter) long multihull originally designed by Greg Goodall in 2007 as a non-foiling high-performance multihull [2]. Because of its light and versatile design it was perfectly suited to be converted to a foiling boat. A picture of the Viper while foiling can be found in Fig. 1. The original, non-foiling Viper has -just like regular multihulls- two straight rudders for steering towards the back of the boat and two straight daggerboards as anti-drift mechanism towards the middle of the boat. To enable foiling, a smaller, horizontal symmetric foil is added to the bottom of both rudders to form a T-shaped rudder. Additionally the straight daggerboards are replaced by a Z-shaped daggerboard. A picture of this setup can be found in Fig. 2. The vertical *stem* of the rudder will from here on be called the *rudder*, the horizontal symmetric foil at its bottom the *elevator* and the daggerboard the *Z-board*. The principle of the setup of the Viper (and other foilers) is very similar to that of a regular airplane. The two Z-boards provide the necessary lift near the centre of gravity, the two elevators are placed further downstream to enable stable flight, and the two rudders are there both for active steering and directional stability.

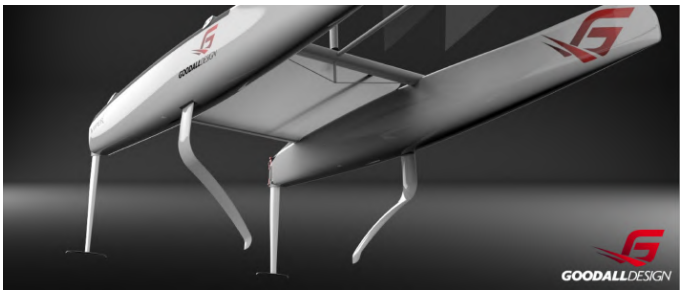

Fig. 2. Details of the Vipers foils.

II. Stability Dynamics

The dynamic stability analysis is used to compare the stability of different geometries or conditions. This analysis also allows to predict the dominant motions the boat will experience. As the literature on hydrofoil boat dynamic stability is rather limited and the principle of a hydrofoil boat is similar to that of an airplane, the stability analysis is based on the theory developed for airplanes. This theory is described in many works, such as Drela's work on "Flight Vehicle Aerodynamics". A lot of inspiration came from this book. One of the only sources on dynamic

stability analysis specifically for hydrofoil boats is the work by Masuyama [4]. In this section a theory is developed based on these two sources, which is suited specifically for the case under consideration.

A. General approach

There are 12 equations governing the motion of the boat: 6 kinematic equations and 6 dynamic equations. These 12 equations are used to solve 12 *motion variables*. The *state-vector* $S(t)$ is a combination of these 12 motion variables and contains consecutively the position, rotation, velocity and angular velocity of the boat.

$$S(t) = \{x\ y\ z\ \phi\ \theta\ \psi\ u\ v\ w\ p\ q\ r\}^T$$

The boat is assumed to experience a small disturbance from an original equilibrium state. Due to this disturbance, every term in the 12 equations is substituted for its equilibrium term (denoted with subscript 0) plus a deviation from this equilibrium value (denoted as a Δ term). This is demonstrated in Eq. 1 for the vertical position z. This allows to linearize the equations.

$$z(t) = z_0 + \Delta z(t) \tag{1}$$

Forces and moments are functions of the flow-field around the boat. In order to make the equations of motion tractable they are assumed to be a function of the 12 motion variables. The forces and moments can then be approximated using a first-order Taylor expansion. This is demonstrated in Eq. 2 for the longitudinal horizontal force ΔX:

$$\Delta X = \sum_i \frac{\partial X}{\partial a_i} \Delta a_i \tag{2}$$

$$\text{with } a = x, y, z, \phi, \theta, \psi, u, v, w, p, q, r$$

The individual derivatives in this expression are called the *stability derivatives*, some can be omitted depending on the situation. Using the state-vector $S(t)$, a matrix notation for the eq. of motion can be found. This is shown in Eq. 3 where A is the stability matrix and contains the stability derivatives. In the context of an airplane this matrix would be composed of three decoupled subsets: a *longitudinal*, a *lateral* and a *navigational* subset [3].

$$\frac{d}{dt} S(t) = A \cdot S(t), \quad A \in \mathbb{R}^{12\times 12} \tag{3}$$

Due to the presence of the water surface and the sail, the stability matrix of a hydrofoil boat has a different form. The draft z, has an effect on all three subsets, whereas all the derivatives to z would be zero in the case of an airplane. This can easily be understood: An airplane could fly e.g. 10 m higher or lower, but this would not affect any force or moment. If the Viper from Fig. 1 would be lowered a certain distance, a larger part of the Z-boards would be submerged and this would consequently influence all force and moment terms.
Since there usually is a misalignment between the propulsive force of the sail and the longitudinal direction of the boat, the boat will experience a certain heel ϕ_0 and sideslip v_0. The decoupling characteristic between the different subsets of the stability matrix would cease to be valid, as a perturbation of any form would simultaneously affect longitudinal and lateral motions. However, as the boat is meant to be sailed without any heel (this is the most efficient, i.e. fastest, way of sailing), the heel is assumed to be zero. In addition, the sideslip is very small compared to the forward velocity u_0 and will also be neglected.

B. Simplifications

To reduce the complexity of the problem, certain simplifications can be made based on the stability analysis. The intended results should somewhat justify the used resources. A two-phase simulation where the whole boat is included, would lead to more accurate results, but also to an unreasonably large mesh and calculation time. Therefore, it was chosen to only model the rudder, the elevator and the Z-board below the water surface and to assume that all forces and moments above the water surface are constant. In reality this would however not be true. The biggest contribution above the water originates from the sail, e.g. the sail leads to a large variation in experienced force and moment when rolling, $p \neq 0$. The sail consequently has a large contribution to the force and moment derivatives to the roll motion.
This immediately leads to another simplification: only *longitudinal* motions are considered: motions along the x- and z-axis and a rotation around the y-axis. This is due to the fact that the *lateral* motions are heavily affected by the sail which is modelled as a constant force and moment. The rotations around the z-axis are more of interest for a directional stability analysis. The assumption that all forces and moments above the water surface are constant is in the case of longitudinal motion justified. The effect on the sail of changing the draft or the trim angle will be next to none.

C. Longitudinal stability model

As this model considers only one rotation, the use of the inertial earth-bound frame is more convenient than the usual stability frame, to write the governing equations of motion. A view of the mentioned axis systems can be found in Fig. 3. The axis system in uppercase ($X^eY^eZ^e$) is the earth-bound right-handed axis system. The other frame is called the stability frame ($x^{b'}, y^{b'}, z^{b'}$), it is displayed in orange. Its origin is coincident with the centre of gravity and the speed in equilibrium conditions lies in the xy-plane. The Z-axis is chosen downwards, as this is conventional in maritime engineering.

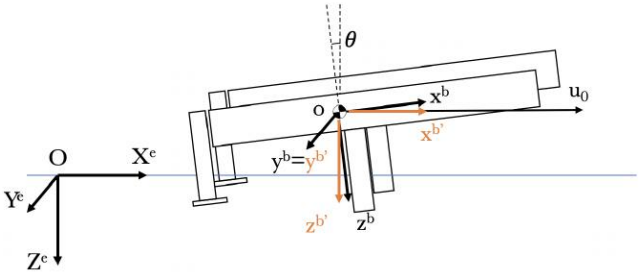

Fig. 3. An overview of the used axis systems.

As only longitudinal motions are considered, the 6 dynamic relations of the general approach mentioned in Sec. II-A are reduced to only 3 relations: force balances along the X and Z direction and a moment balance around the y-axis. The moment of inertia I_{yy} and moment M are defined around the centre of gravity. These 3 dynamic relations are completed with 2 kinematic relations as is shown in Eq. 4.

$$\begin{cases} F_x = m\dot{u} \\ Z = m\dot{w} \\ M = I_{yy}\ddot{\theta} \\ w = \dot{z} \\ q = \dot{q} \end{cases} \Leftrightarrow \begin{cases} \dfrac{du}{dt} = \dfrac{F_x(u,z,\theta)}{m} \\ \dfrac{dw}{dt} = \dfrac{Z(u,z,\theta)}{m} \\ \dfrac{dq}{dt} = \dfrac{M(u,z,\theta)}{I_{yy}} \\ \dfrac{dz}{dt} = w \\ \dfrac{d\theta}{dt} = q \end{cases} \tag{4}$$

The above equations are linearized using small-disturbance theory, and the forces and moment are substituted for their Taylor approximations as in Eq.2. Eq. 5 is then obtained with the stability matrix A defined in Eq. 6.

$$\frac{d}{dt}\begin{bmatrix} \Delta u \\ \Delta z \\ \Delta\theta \\ \Delta w \\ \Delta q \end{bmatrix} = [A] \cdot \begin{bmatrix} \Delta u \\ \Delta z \\ \Delta\theta \\ \Delta w \\ \Delta q \end{bmatrix} \tag{5}$$

$$[A] = \begin{bmatrix} \frac{1}{m}\frac{\partial X}{\partial u} & \frac{1}{m}\frac{\partial X}{\partial z} & \frac{1}{m}\frac{\partial X}{\partial \theta} & \frac{1}{m}\frac{\partial X}{\partial w}^{*} & \frac{1}{m}\frac{\partial X}{\partial q}^{**} \\ 0 & 0 & 0 & 1 & 0 \\ 0 & 0 & 0 & 0 & 1 \\ \frac{1}{m}\frac{\partial Z}{\partial u} & \frac{1}{m}\frac{\partial Z}{\partial z} & \frac{1}{m}\frac{\partial Z}{\partial \theta} & \frac{1}{m}\frac{\partial Z}{\partial w}^{*} & \frac{1}{m}\frac{\partial Z}{\partial q}^{**} \\ \frac{1}{I_{yy}}\frac{\partial M}{\partial u} & \frac{1}{I_{yy}}\frac{\partial M}{\partial z} & \frac{1}{I_{yy}}\frac{\partial M}{\partial \theta} & \frac{1}{I_{yy}}\frac{\partial M}{\partial w}^{*} & \frac{1}{I_{yy}}\frac{\partial M}{\partial q}^{**} \end{bmatrix} \tag{6}$$

D. Derivatives

The stability derivatives to w and to q are very expensive to calculate using CFD as they require transient simulations. Nevertheless, their influence on the eigenmodes of the stability matrix cannot be understated. Neglecting them would lead to meaningless results. This hypothesis was supported by the numerical stability derivatives as provided by Masuyama [4] and later also confirmed by the stability analysis of the Viper. The terms denoted by (*) and (**) will rather be approximated using the other 9 derivatives which have been calculated in the stability matrix A from Eq. 6 using only steady-state simulations.

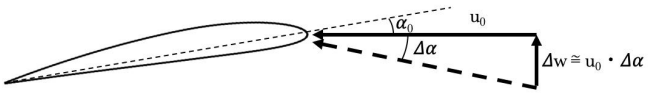

Fig. 4. Effect of the vertical velocity, w.

The terms denoted with (*) in Eq. 6 are the force and moment derivatives to the speed in the vertical direction (heave). These terms will be approximated using the derivatives to the trim angle θ: $\frac{\partial X}{\partial \theta}$, $\frac{\partial Z}{\partial \theta}$ and $\frac{\partial M}{\partial \theta}$. As can be seen from Fig. 4 a perturbation Δw of the vertical velocity causes a change in angle of attack α from the viewpoint of the foils. Since a hydrofoil boat sailing in equilibrium conditions will always have a horizontal speed, a change in trim angle $\Delta\theta$ is seen by the foils as a change in angle of attack $\Delta\alpha$. The difference between changing α and changing θ lies in the fact that the submerged area differs in the case the trim angle is changed. This effect is rather small and can be neglected, i.e. $\frac{\partial ...}{\partial \theta} \sim \frac{\partial ...}{\partial \alpha}$. Assuming small disturbances around an equilibrium point, $\frac{\partial Z}{\partial w}$ can be approximated as is shown in Eq. 7. The procedure for $\frac{\partial X}{\partial w}$ $\frac{\partial M}{\partial w}$ is analogous.

$$\frac{\partial Z}{\partial w} = \frac{\partial Z}{\partial \theta}\frac{\partial \theta}{\partial w} \approx \frac{1}{u_0}\frac{\partial Z}{\partial \theta} \tag{7}$$

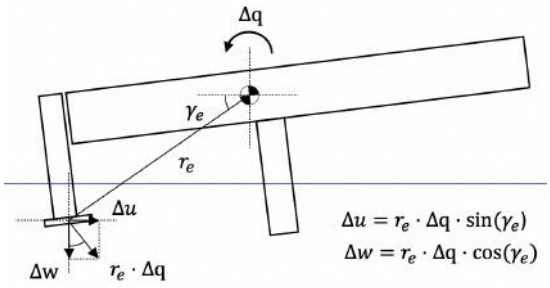

Fig. 5. Effect of the pitch, q.

The terms denoted with (**)in Eq. 6 are the derivatives of the force and moment to pitch. An angular velocity q around the centre of gravity causes an additional velocity component on both foils. This velocity component can be decomposed in a horizontal and vertical part, respectively Δu and Δw, as is demonstrated in Fig. 5. This component depends on the individual positioning of each foil. The positioning is characterized in the figure by the distance to the centre of gravity r_e and the angle in the stability frame to the horizontal plane, γ_e. Using the expression from Eq. 7 an approximation of $\frac{\partial M}{\partial q}$ is developed in Eq. 8. The procedure for X and Z is analogous.

$$\begin{aligned} \frac{\partial M}{\partial q} &= \frac{\partial M}{\partial u}\frac{\partial u}{\partial q} + \frac{\partial M}{\partial w}\frac{\partial w}{\partial q} \\ &= \frac{\partial M}{\partial u} r_e \sin(\gamma_e) + \frac{\partial M}{\partial w} r_e \cos(\gamma_e) \\ &\approx \frac{\partial M}{\partial u} r_e \sin(\gamma_e) + \frac{1}{u_0}\frac{\partial M}{\partial \theta} r_e \cos(\gamma_e) \end{aligned} \tag{8}$$

Notice that this procedure has to be completed for every component separately as their individual positioning varies. Afterwards their individual derivatives are summed to obtain the total derivative necessary in the stability matrix.

These approximations for the derivatives are quite valuable as it allows to construct the stability matrix A with only a few steady-state simulations.

III. CFD Methodology

A. Mesh

The complete mesh will be constructed using *overset*. Oversetting allows us to create three much 'simpler', separate component meshes together with a rectangular hexahedral background mesh in which they overlap. The solver will, after initialization, remove overlap between the different meshes by deactivating redundant cells. The background mesh can be much coarser than the component meshes as nearly no gradients will be present here. Nevertheless, special care should be taken to make sure that component meshes and background mesh have similar sizing in regions of overlap as this will give rise to better results for the overset initialization.

Assuming a symmetric boat experiencing only *longitudinal* motions, the used geometry should only contain one half boat. This results in 1 rudder, 1 elevator and 1 Z-board as our geometry. Simulating only half of the geometry has a large beneficial influence on calculation time. The CAD-files of the Viper were provided by Goodall Design. Using these CAD-files, the three components (rudder, elevator and Z-board) are meshed separately using the *ICEM* software package from *ANSYS*. An example of a component mesh is shown in Fig. 6 for the elevator.

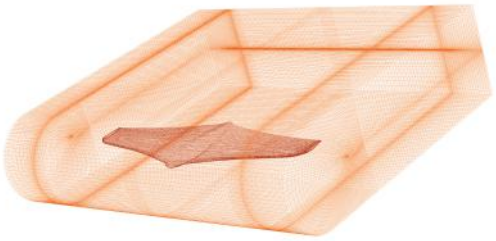

Fig. 6. The elevator mesh.

A fourth mesh contains a much larger surrounding background in which the three other meshes are combined using the overset functionality from *FLUENT*. The three component meshes are all hexahedral C-grid meshes which are sufficiently long downstream to resolve the wake. The C-grid has a radius of only 1 chord length. The first cell of the boundary layer of all three foils is located at $0.1\ mm$ to have a y^+ value approximately between 30 and 300. An overview of the components together with the background mesh is shown in Fig. 7. It can be seen how the background mesh is refined towards the components. It was chosen to model the free surface as a *rigid lid* rather than using a multi-phase flow method as this is outside the scope of this work. The black surface in Fig. 7 represents the free surface modelled as a free-slip wall. The blue surfaces are pressure outlets which are tilted slightly inwards towards the outlet to prevent reversed flow on these surfaces. The green surface, which lies at the centre line of the boat, is modelled as a symmetry plane. This background mesh is completed with a velocity inlet and pressure outlet at the ends which are omitted in the figure.

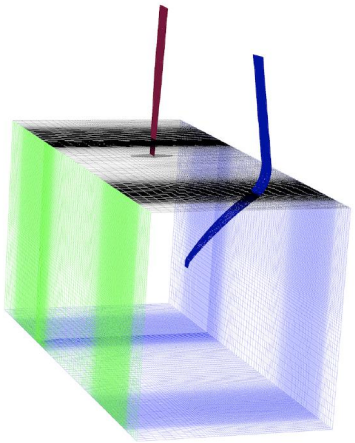

Fig. 7. The components in the background mesh.

B. Flow solver

As the speed range in which foiling is to be expected lies above $5\ m/s$ and the foils have chord lengths of $0.2\ m$, Reynolds numbers always lie well above 10^6. Turbulence is modeled using the $k-\omega\ SST$ model. At the velocity inlet the turbulence intensity is set to 1% and the viscosity ratio $\frac{\mu_t}{\mu}$ is set to 1, similar to what was found accurate by Lopes [5]. To include the effects of hydrostatic pressure gravity g is enabled and a hydrostatic pressure profile is imposed at the pressure outlets. The different components can be rotated and translated separately to create different setups. The standard geometry has a rudder rake of $-1°$ and a foil rake of $4°$. The rake is the relative angle of a foil to the boat.

C. Equilibrium state

As only forces and moments resulting from the foils below the water surface are calculated, other forces and moments should be estimated in order to find a realistic equilibrium state of the boat. For the force balance the weight of boat ($140\ kg$) together with the weight of the crew ($140\ kg$) should be included. As only half of the boat is modelled, only half of the weight is included, resulting in a downwards force of $1.37 \cdot 10^3\ N$. The moment generated by the sail also has to approximated. The drag generated by the foils follows from the CFD calculations, e.g. the drag generated at forward speed of $10\ m/s$ is equal to $215\ N$. The sail should deliver a force which is equal in magnitude but opposite in direction to this drag. Data provided by Goodall Design shows that the point of application of the sail lies $3.25\ m$ above the centre of gravity. From this the force and its point of application the moment can be calculated.

An algorithm to determine the equilibrium state for an arbitrary geometry and conditions was developed. A geometry can vary by changing the rudder rake, foil rake, the CoG, ... A setup can change by varying the speed of the boat. The goal of the algorithm is to find a relative trim angle $\Delta\theta$ and relative draft Δz at which both the total moment and total force on the boat are zero. This trim angle and draft are defined in reference to an arbitrary initial orientation. The algorithm is based on the

Newton-Rhapson root-finding method for 2 variables in which the new position is iteratively calculated based on the force and moment.

$$\begin{bmatrix}\Delta z_k \\ \Delta\theta_k\end{bmatrix} = J^{-1}\begin{bmatrix}-F_k \\ -M_k\end{bmatrix},\ J = \begin{bmatrix}\frac{\partial Z}{\partial z} & \frac{\partial Z}{\partial \theta} \\ \frac{\partial M}{\partial z} & \frac{\partial M}{\partial \theta}\end{bmatrix} \tag{9}$$

In every step the 4 components of the Jacobian J are calculated. However if both draft and trim angle are updated simultaneously, there is no way of calculating the derivatives, as their individual contributions cannot be distinguished. That is why a segregated approach is proposed. Every iteration consists of two sub-iterations: one sub-iteration for the draft update Δz and one for the trim angle update $\Delta\theta$. Based on the Jacobian J_k an update for the draft and trim are calculated, Δz_k, $\Delta\theta_k$. In iteration $k+\frac{1}{2}$ the position of the boat is updated with Δz_k. The flow for this new orientation is solved and from the resulting new force and moment, $Z_{k+\frac{1}{2}}$ and $M_{k+\frac{1}{2}}$, the derivatives to z are updated. In iteration $k+1$ the position of the boat is updated with $\Delta\theta_k$. The flow for this new orientation is solved and from the resulting new force and moment, Z_{k+1} and M_{k+1}, the derivatives to θ are updated as well. Using the Jacobian J_{k+1} new updates are calculated and the algorithm is re-iterated. This gets demonstrated in Eq. 10.

$$\begin{aligned}
&① \begin{bmatrix}\Delta z_k \\ \Delta\theta_k\end{bmatrix} = J_k^{-1}\begin{bmatrix}(-Z)_k \\ (-M)_k\end{bmatrix} \\
&② \text{ simulate } (z_k+\Delta z_k, \theta_k) \Rightarrow (Z_{k+\frac{1}{2}}, M_{k+\frac{1}{2}}) \\
&\quad \rightarrow \frac{\partial Z}{\partial z} = \frac{Z_{k+\frac{1}{2}}-Z_k}{\Delta z_k};\frac{\partial M}{\partial z} = \frac{M_{k+\frac{1}{2}}-M_k}{\Delta z_k} \\
&③ \text{ simulate } (z_k+\Delta z_k, \theta_k+\Delta\theta_k) \Rightarrow (Z_{k+1}, M_{k+1}) \\
&\quad \rightarrow \frac{\partial M}{\partial \theta} = \frac{M_{k+1}-M_{k+\frac{1}{2}}}{\Delta\theta_k};\frac{\partial Z}{\partial \theta} = \frac{Z_{k+1}-Z_{k+\frac{1}{2}}}{\Delta\theta_k} \\
&④ \begin{bmatrix}\Delta z_{k+1} \\ \Delta\theta_{k+1}\end{bmatrix} = J_{k+1}^{-1}\begin{bmatrix}(-Z)_{k+1} \\ (-M)_{k+1}\end{bmatrix} \ \ldots
\end{aligned} \tag{10}$$

The algorithm was implemented in FLUENT making use of *journal files* together with *UDFs* (User-defined functions).

D. Derivatives

Once the equilibrium state for a geometry and setup is found, the stability matrix needs to be constructed. The calculations for the derivatives, necessary for constructing the stability matrix, are straightforward. They are calculated with a one-sided finite difference around the equilibrium state. Together with the forces and moment from the equilibrium state (which are approximately zero), three additional sets of the forces and moment are calculated for disturbances in respectively draft, trim adn surge. This is demonstrated in Eq. 11:

$$\frac{\partial A}{\partial a} = \frac{A_{\Delta a}-A_0}{\Delta a}, \quad A = X, Z, M, \quad a = \theta, z, u \tag{11}$$

with A_0, the force or moment from the equilibrium state and $A_{\Delta a}$ the force or moment from the perturbed state.

IV. Results

The following section presents the results for the standard geometry, with an elevator rake of $-1°$ and a Zboard rake of $4°$, at a speed of $10\ m/s$.

A. Equilibrium state

The equilibrium state was calculated from an arbitrary starting state. This starting state has a zero trim angle and a draft where the rudder is submerged $100\ mm$ and the Z-board $400\ mm$. The position of the resulting equilibrium state relative to this starting state is defined by $\Delta z = 159\ mm, \Delta\theta = -2.38°$. This means that the boat moves deeper into the water and is tilted slightly *nose-down*. The rudder is now submerged $260\ mm$ and the Z-board$560\ mm$.

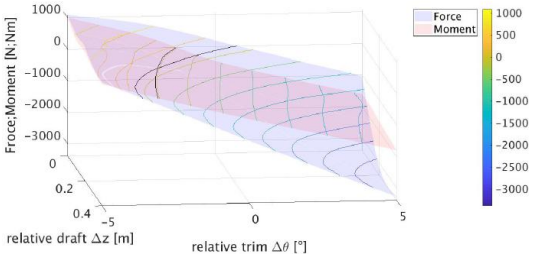

Fig. 8. A surface plot of the of the force and moment of the Viper as a function of the relative draft z and the relative trim angle θ.

In Fig. 8 a surface plot is shown of the force Z and moment M as a function of the relative draft and trim. Notice that as the Z-axis is directed downwards, a *lift*-force is negative and a boat which lies deeper in the water has a more positive draft. It can be observed how the moment M depends primarily on the trim but that the force Z depends on both the trim and the draft. The two black iso-curves represent the states where the force Z or the moment M is zero. The location where the two curves intersect, is the location of the equilibrium state.

B. Stability matrix

Using finite differencing, the individual derivatives of the three components are calculated for the draft z, trim θ and surge u. These derivatives are then used to construct the stability matrix A for the standard geometry sailing at a speed of $10\ m/s$:

$$[A] = \begin{bmatrix}-0.27 & -2.21 & -4.99 & -0.50 & 0.00 \\ 0 & 0 & 0 & 1 & 0 \\ 0 & 0 & 0 & 0 & 1 \\ -2.24 & -57.20 & -156.21 & -15.62 & -6.51 \\ 0.01 & -6.42 & -78.59 & -7.86 & -14.75\end{bmatrix}$$

Using *MATLAB*, the eigenvalues and eigenvectors of this matrix can be determined. The eigenvalues determine the general behaviour of each mode, and the eigenvectors will determine the amplitude and phase of each variable. The eigenvalues are visualised in Fig. 9 and the eigenvectors are visualised in Fig. 10,11 and 12. From the eigenvalues and eigenvectors, the eigenmodes can be constructed:

$$\Delta x_i = v_i e^{\lambda_i t} \qquad \text{with } i = 1, ..., 5 \tag{12}$$

From the eigenvalues some interesting conclusions can be drawn. The first thing which can be noted is that they all have a negative real part, meaning that the boat is *dynamically stable*. Furthermore there is one real eigenvalue and two complex conjugated pairs.

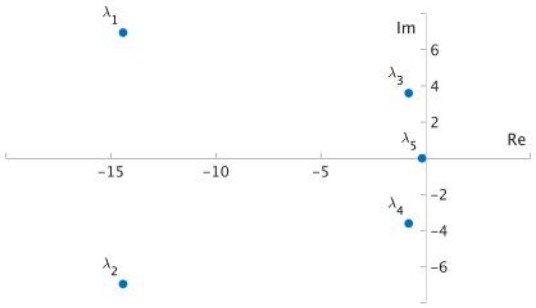

Fig. 9. The root locus diagram for the standard geometry sailing at a speed of $10\ m/s$.

Taking a look at the real eigenvector v_5 in Fig. 10, some characteristics of the behaviour of the eigenmode Δx_5 can be recognized. An increase in speed Δu is associated with a decrease in draft Δz (meaning that the boat gets lifted from the water). This corresponds to the behaviour that is expected. A draft variation Δz occurs naturally together with a heave variation Δw. As this is a real mode, this draft variation damps out without any overshoot. A half-life $t_{\frac{1}{2}}$ is the time needed for the value to decrease by $\frac{1}{2}$ times its original value (exponential decay). From the half-lifes it can be seen that it will take $3.89\ s$ for this mode to damp out. This means the boat will react quite slowly.

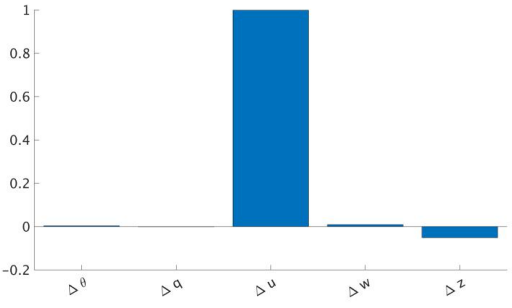

Fig. 10. A visualisation of the real eigenvector v_5.

The combination of the eigenmodes Δx_1 and Δx_2 will be a heavily damped, sinusoidal motion dominated by a variation in heave Δw and pitch Δq. This resembles some kind of wobbling. After the boat moves downwards, it starts to tilt nose-up. This results in more lift, meaning that the boat eventually starts moving up again. Hence the oscillatory motion. The heave and pitch motion are almost in phase with each other. This mode has a half-life $t_{\frac{1}{2};1} = t_{\frac{1}{2};2} = 4.81 \cdot 10^{-2}\ s$ and a period $T_1 = T_2 = 0.904\ s$.

The combination of eigenmodes Δx_3 and Δx_4 will be a weakly damped, sinusoidal motion, again dominated by a variation in heave Δw and pitch Δq. The half-life is $t_{\frac{1}{2};3} = t_{\frac{1}{2};4} = 8.54 \cdot 10^{-1}\ s$ and the period $T_3 = T_4 = 1.75\ s$. As the half-life and period are larger in this case, the variation in trim angle $\Delta\theta$ and draft Δz resulting from the variation in heave and pitch will be more outspoken. This is demonstrated by the larger vector components for trim and draft in Fig. 12.

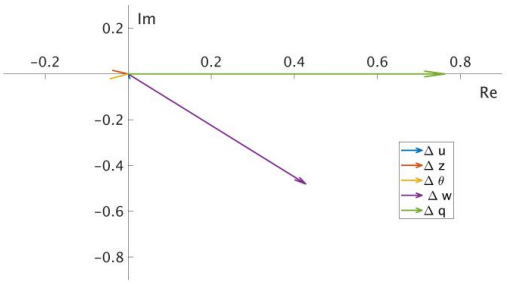

Fig. 11. A visualisation of the complex eigenvector v_1.

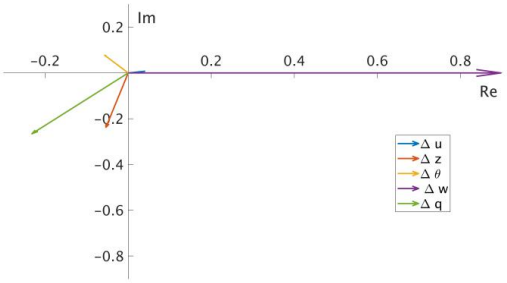

Fig. 12. A visualisation of the complex eigenvector v_3.

V. Conclusions

A framework for quantifying the longitudinal stability of a hydrofoil boat has been developed. This framework was applied to the Viper, from which could be concluded that this design is dynamically stable. This is also supported by full scale tests. Dynamic stability analysis of a hydrofoil boat using CFD is a rather new application and looks promising, but of course it needs improvement to reap all the benefits. For future work it can be of interest to perform the stability analysis for more geometries than one to be able to compare the stability and check if the same modes reoccur. Having a more accurate model for the sail forces will allow to include lateral motions as well, to have a more complete stability analysis. Experimental data from towing tanks or full-scale tests is also key for future development of this technique.

References

[1] E. Bunting. (2015). *Franck Cammas airlifted with serious injury*, Yachting World. https://www.yachtingworld.com/news/french-americas-cup-skipper-franck-cammas-badly-injured-after-being-run-over-by-foiling-catamaran-69178, April 2019

[2] World Sailing. (2010). *Viper: Classes and equipment*. https://www.sailing.org/classesandequipment/VIP.php, April 2019.

[3] M. Drela. *Flight Vehicle Aerodynamics*. MIT Press, 2014.

[4] Y. Masuyama. "Stability analysis and prediction of performance for a hydrofoil sailing boat. Part 2: Dynamic stability analysis" *International Shipbuilding Progress*, 34:20-29,1987.

[5] R. M. A. Lopes. Calculation of the flow around hydrofoils at moderate Reynolds numbers. Lisboa Instituto Superior Tecnico, 2015.

Contents

List of Figures

List of Tables

Nomenclature

List of Abbreviations

2D	2-dimensional
3D	3-dimensional
AC	America's Cup
AoA	Angle of Attack.
BL	Boundary Layer
CFD	Computational Fluid Dynamics
CoG	centre of gravity
GUI	Graphical User Interface
LE	Leading edge
ODE	Ordinary differential equations
TE	Trailing Edge
TUI	Text User Interface
UDF	User-Defined Function

List of Greek Symbols

α	angle of attack
ϵ	angle of the bottom sail to the centre line of the boat
γ_T	angle of the true wind to the centre line of the boat

$\gamma_{el}^{b'}$	the angle of the elevator to the CoG in the stability frame around the y-axis
Ω	angular velocity vector
ω	turbulent dissipation rate
ϕ, θ, ψ	Euler angles: heel, trim and heading

List of Roman Symbols

$\overline{\overline{I}}^{b'}$	inertia tensor of the boat defined in the stability axes.
A	stability matrix
C_D	drag coefficient
C_L	lift coefficient
k	turbulent kinetic energy
L, M, N	the moments around the different axes
M_{sail}	the moment generated by the sail
p, q, r	pitch, roll and yaw
R_0	position vector of the CoG
$r_{el}^{b'}$	the distance of the elevator to the CoG in the stability frame
S_x, C_x	sin(x) and cos(x)
$t_{1/2}$	half-life
U	velocity vector
u, v, w	surge, sway and heave
U_{ST}	true wind speed
X, Y, Z	the forces along the different axes
x, y, z	x-pos., y-pos. and draft
$x^b,\ y^b,\ z^b$	body-fixed frame

$X^e,\ Y^e,\ Z^e$	Earth-bound frame
$x^{b'},\ y^{b'},\ z^{b'}$	stability frame
X_z, ...	the X-force derived to the draft z, ...
$\mathrm{F}^{b'}$	force matrix in the stability frame
g	gravitational constant
m	mass of the complete boat+crew
$\mathrm{M}^{b'}$	moment matrix in the stability frame
X(t)	state vector
X_0	equilibrium state

List of Subscripts and Superscripts

$\ddot{\phi}$	derivative to roll accel. $\ddot{\phi}$
$\ddot{\theta}$	derivative to pitch accel. $\ddot{\theta}$
$\dot{\phi}$	derivative to roll $\dot{\phi}$
$\dot{\theta}$	derivative to pitch $\dot{\theta}$
$\dot{u}$	derivative to surge accel. $\dot{u}$
$\dot{v}$	derivative to sway accel. $\dot{v}$
$\dot{w}$	derivative to sway accel. $\dot{w}$
ϕ	derivative to heel ϕ
θ	derivative to trim θ
u	derivative to surge u
v	derivative to sway v
w	derivative to heave w
z	derivative to draft z

0	equilibrium values
b	features referenced in the body-fixed frame
b’	features referenced in the stability frame
e	features referenced in the earth-bound frame

1 Introduction

1.1 Background

Sailing is one of the oldest ways of transport used by humankind. Earliest clues of sea-going vessels under sail were as early as 5000 BC [7]. Before the industrial revolution sailing vessels were the only way of travelling across oceans and seas and were therefore one of the main drivers in trade, exploration and industry. Due to the inventions of alternatives to provide propulsion, sailing lost a lot of its relevance. Ships were no longer restricted by the presence or the direction of wind. Today, under influence of climate change there is an urgency to find sustainable solutions in the transport sector which could very well lead to a renaissance of sailing in industry. As the relevance of sailing in industry faded, sailboat racing has been one of the main drivers in development within sailing. Mainly the America's Cup has played a big part in the "recent" development. The America's cup is the oldest trophy in sports which is still contested today[8], the cup dates back to 1851. Under the influence of the America's Cup, sailing yachts have seen big technological advances in various domains (sails, materials, appendages, hulls, ...). It can be compared to the contribution of Formula 1 racing to the car industry. One of the most recent developments is the introduction of hydrofoils, which allow a sailing yacht to hover/fly above the water by generating an upwards force. The hydrofoils lift the complete hull of the yacht out of the water which greatly reduces the resistance and therefore allows for greater sailing speeds. The working principles of hydrofoils and sailing yachts in general will be explained later on.

1.2 Goodall Design Viper and motivation

The introduction of hydrofoils at the highest level of the sport demonstrated their advantages and how exciting they can be to a wider audience. This was the trigger for Goodall Design, an Australian company building and designing multihulls (catamarans), to try and make this technology available to everyone by converting their already existing platform the Viper to a foiling version. The Goodall Design Viper (from now on simply "Viper") is a multihull class which was devised in Australia by Greg Goodall in 2007 [9]. The Viper is a relatively light and nimble boat of 5 meters long (16 feet) and therefore lends itself perfectly to be upgraded to a foiling version. Because of its light construction the Viper always has been a versatile platform that can be sailed by lighter youth teams, mixed teams and even solo sailors. In Fig. 1.1 multiple vipers can be seen while racing.

Figure 1.1: Multiple GD Vipers seen racing. ©Jasper van Staveren

1.3 Goal

Both in the America's Cup and in the Olympics development of hydrofoils is focused on decreasing drag and increasing lift to allow for greater speeds. The intrinsic tendency to maintain the equilibrium position is of secondary importance, as there are often control systems present

with feedback loops to provide the necessary stability. A sailing yacht which is foiling with its hull lifted out of the water experiences a great reduction in stability as the stability is no longer provided by the buoyant forces of the hull but rather by the lifting forces of the hydrofoils. The Viper is however a smaller and much simpler yacht without any control systems and thus should be inherently stable. Stability has become very important to Goodall Design as they want to make this technology accessible to everyone, even the less experienced amateur. The goal of this thesis is to find a way to quantify stability of a foiling catamaran.

1.4 Structure

The first 4 chapters of this thesis cover the theoretical backbone and literature review. Chapter 2 is put in place to have some background in both sailing as hydrofoiling. Chapter 3 handles the literature on stability dynamics. It comprises a section on airplane stability dynamics as the similarities between airplanes and hydrofoiling boats are rather striking. In chapter 4 the used model will be discussed in more detail. The methodology will be handled as a whole in chapter 5. Chapter 6 will tackle the results of the simulations and will lead up to conclusions in chapter 7.

2

Hydrofoils & Sailing

This chapter provides the reader with the necessary knowledge both about sailing and hydrofoiling, as this is deemed necessary to understand this work. The physics provided here are based on C. A. Marchaj's *Aero-hydrodynamics of sailing* [10].

2.1 Sailing

2.1.1 Background

Pressure differences throughout the atmosphere result in flows of air which we experience as wind. These pressure differences can have various reasons like temperature or humidity and exist at a macro and micro scale: from dominating east-west depressions in the southern ocean to a slight breeze trough a house with its windows opened. This is why wind is present most of the time and nearly everywhere on Earth. Wind possesses large amounts of energy, sometimes even with destructive consequences like with hurricanes or big storms. Sailing is the practice where this wind energy is used to propel a means of transport, most often a yacht.

2.1.2 Principle

The forces on a sailing yacht can be distinguished by means of their origin. The interaction with the air gives rise to aerodynamic forces, the interaction with the water gives rise to hydrodynamic forces. The interplay between these two components will determine if the boat will go forward, sideways or even backwards and will also determine how fast the yacht will be going. A third

force component is caused by the weight of the boat itself and the weight of the crew. As the weight of the boat (140 kg) is usually comparable to that of the two crew members (approx. 2 times 70 kg), the position of the crew consequently has a big influence on the position of the centre of gravity.

Aerodynamic forces The aerodynamic forces are generated by one or more sails. An example of the Viper can be seen in Fig. 2.1. Three sails can be distinguished from left to right: one big sail to the back of the boat called the main sail, a small sail called the jib and a bigger red sail called the gennaker. The last one is only used on particular courses and put away when not beneficial. When having an overhead view of these sails it can be clearly noted that they have an airfoil-like profile. Their shape can be manipulated by controlling the sheets[1]. When these sails are properly trimmed to the wind present and experience a relative motion with the wind, they will generate a force called the total aerodynamic force (see Fig. 2.2). This total aerodynamic force can be decomposed in a driving force along the direction sailed and an aerodynamic side force perpendicular to the direction sailed.

Figure 2.1: An overview of the sails used on the viper. From left to right: main sail, jib and gennaker.

[1] a "sheet" is sailing terminology to term a rope used to control sails

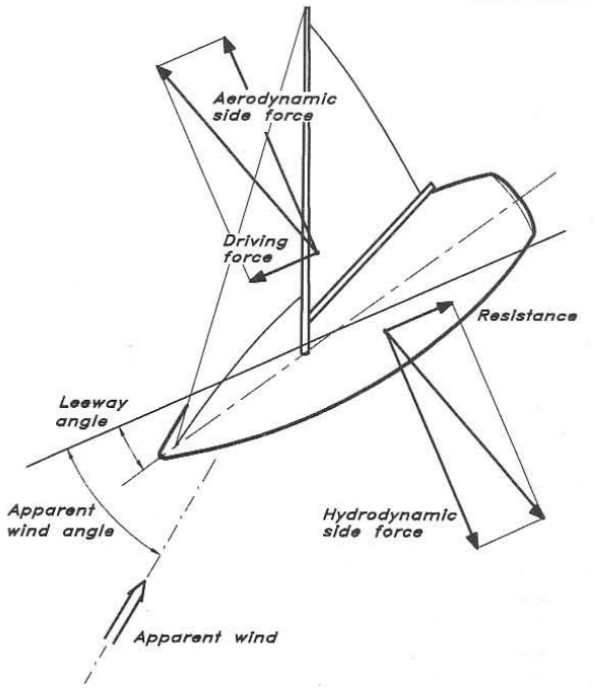

Figure 2.2: The force balance in the XY-plane [1].

Hydrodynamic forces If the boat would generate no other forces, it would just follow the direction total aerodynamic force. However, the hull and appendages will generate a counter-force, called the total hydrodynamic force. This prevents the boat from drifting and consequently forces the boat go straight. The appendages used on a catamaran like the Viper are two rudders at the back of the hulls, and two daggerboards towards the centre of the hulls. In Fig. 2.3 both the rudder and the daggerboard are visible[2]. What happens below the water surface is very similar to what happens above it. If the boat experiences a certain sideways velocity combined with a forward velocity, the rudder and daggerboard will have a certain "angle of attack"[3]. This angle of attack is equal to the leeway angle in Fig. 2.2 and represents what angle the velocity makes to centre line of the boat. The rudders and daggerboards have airfoil-like shapes and will as a result generate a lift opposite to the drift velocity. This is called the total hydrodynamic side-force. Of course will the hull and appendages provide an important resistance as well. The boat will consequently always have a certain sway velocity as this needed to generate a hydrodynamic side force.

[2]It are tweaked versions of this rudder and daggerboard which will later on form the hydrofoils.

[3]An angle of attack represents the angle between a reference line on a foil and the incoming velocity vector.

Figure 2.3: An overview of the hydrodynamic appendages. From left to right: rudder and daggerboard.

In Fig. 2.2 an overview is shown of both the aerodynamic and hydrodynamic forces in the XY-plane. The XY-plane lies perpendicular to the water-surface with its origin in coincident with the CoG. This force balance forms the basis for governing a yacht's speed. The equilibrium between the resistance and driving force determines the forward speed and the equilibrium between the aero- and hydrodynamic side-forces determine the sway velocity. The sway velocity is the velocity of the boat perpendicular to its centre line and parallel with the water-surface.

Other forces As the point of application of the aerodynamic force is located at a certain height above the water-surface and the hydrodynamic force applies below the water-surface, an overturning moment is generated. This is shown in Fig. 2.4. This moment has to be countered by a righting moment to make sure the yacht does not capsize. This righting moment can be generate by various means, e.g. a bulb keel with a yacht, the crew hanging over board with a trapeze line (see Fig. 2.3), ... When the inherent stability and the weight of the crew are not sufficient to prevented capsizing other measures should be taken, e.g. easing the sails.

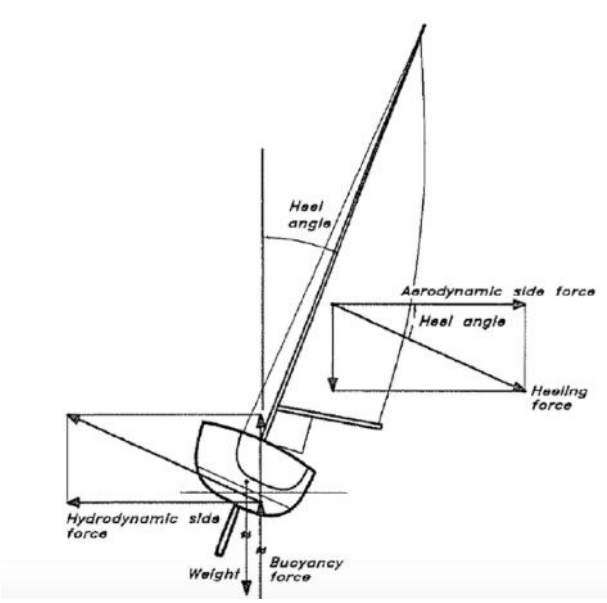

Figure 2.4: The force balance in the YZ-plane [1].

2.2 Hydrofoils

2.2.1 Background

When the aforementioned daggerboards and rudders include a horizontal surface rather than having solely a vertical surface, they are able to provide a vertical force component which can lift the hull from the water. The fascination for the idea of supporting small boats with underwater wings came at the turn of the 19^{th} century with Forlanini and Bell having achieved a successful hydrofoil flight [11]. Other influences came from war-related development during the World Wars. The first real success of hydrofoils in sailing came in 1972 with the design of the catamaran called "ICARUS" by the J Grogono team [10]. This catamaran was however only able to get up onto the foils in a very narrow range of "perfect" conditions (flat water, 15 knots of wind).

The development of low-weight, high-strength materials gave the development of hydrofoils a big boost as the systems could be build equally strong but lighter. One of the most successful classes incorporating hydrofoils has been the "International Moth" class. The Moth is a one-person monohull with a very light construction. The setup consists of a T-shaped rudder acting as a stabiliser and a T-shaped daggerboard acting as a main foil. It differs from the Viper as it has a feedback system for providing stability. In Fig. 2.5 the feedback system can be recognized as the "wand" in front of the boat on the left. This wand registers the distance of the hull above the water-surface and controls a flap on the back of the main foil and adjusts this flap according. This way it can also react to incoming waves as the wand is placed upstream.

Figure 2.5: The international moth with feedback system for stability [2].

The introduction of hydrofoiling to a wider audience can be attributed to the America's Cup in 2013 [8]. Back then the AC was sailed on big foiling catamarans, with T-shaped rudders and L-shaped daggerboards. They used a "3-point foiling system", which means that the windward[4] main foil is lifted from the water when sailing in a straight line. This is done to avoid creating lift which increases the overturning moment mentioned before. They were sailed with one of the crew members on board constantly adjusting the "rake"[5] of both the main foils and the stabilizers to achieve stable flight.

Figure 2.6: The AC72 of Oracle Team USA in action before the America's Cup of 2013 on San Francisco Bay [3].

The 3-point foiling system set-up was also tried on smaller catamarans like the "Flying Phan-

[4]Windward is the side from which the wind blows, it is the opposite of leeward.
[5]The rake is the angle of the hydrofoils

tom" which is an 18 foot catamaran. However, the fact that during manoeuvres the main foils had to be lowered and lifted from the water was rather intensive for the two-person crew to manage. As a remedy the "4-point foiling system" was conceived. In this system both foils were smaller and the windward foil no longer had to be lifter from the water. The first classes to use this 4-point system was the one-person A-class catamaran and the two-person Narca 17 MKII. The Nacra will be the catamaran sailed at the Olympic Games of Tokyo 2020.

2.2.2 Principle & controls

The 4-point foiling system is also used for the Viper Foiling, as it lends itself very well to an easy foiling experience as the foils don't have to be lowered and raised with every manoeuvre. The foiling system makes use of two T-shaped rudders and two Z-shaped daggerboards as can be seen in Fig. 2.7. The stability in the vertical direction is provided by the diagonal orientation of the Z-foil. This can be explained as follows: if the lift generated by the foils is higher than the weight of crew and boat combined, the boat will rise out of the water. This decreases the lift-generating surface until the lift balances out downward oriented forces. The opposite happens when the lift is lower.

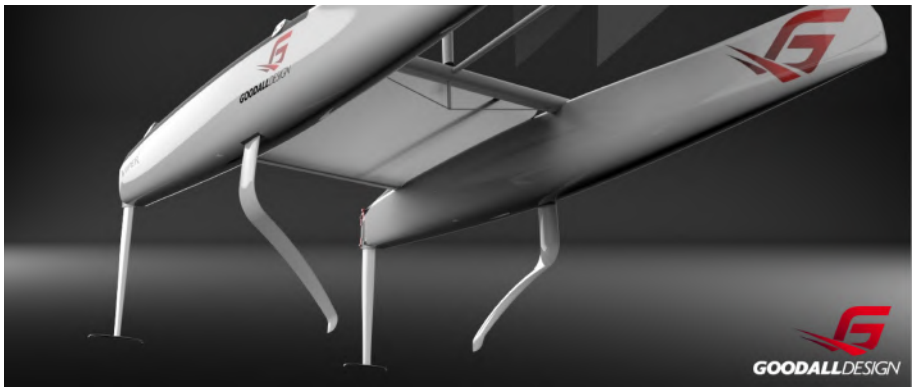

Figure 2.7: The foil setup used for the Viper Foiling.

An important control parameter is the angle at which both the main foil and the stabilizer are set up as these will determine the ease of take-off and the stability and speed during flight. A more positive rake on the main foil is used in lower speed regions were more lift is needed to raise the hull from the water. At higher speeds less rake is needed on the main foils to achieve this. Adjusting the rake of the main foil can be done while sailing, so it happens that the rake is lowered after the boat has taken off as it will now have a higher speed. Lowering the rake will also allow for higher speeds as drag usually decreases with lower angles of attack. The rake of the stabilizers can only be adjusted ashore, as this requires a wrench. Another important parameter to control flight characteristics is the position of the centre of gravity, which can be adjusted by movement of the crew across the boat. Often the crew will move backwards when

the boat is still in floating-mode to increase the angle of attack which as a result will increase the lift to aid in take-off. Floating mode will be used to describe the condition when the hull is not lifted from the water and buoyancy of the hull still accounts for a significant part of the upward forces.

3

Stability Dynamics

This chapter forms the theoretical basis for quantifying the stability of a hydrofoil boat. When looking at the set up of the Foiling Viper and other hydrofoiling boats, lots of similarities can be found with airplanes. Both setups make use of a big lifting-surface, that is located near the CoG , which is mainly responsible for providing the necessary lift and a second, smaller lifting-surface located further downstream responsible for stability. These similarities and the lack of relevant literature, that deals specifically with hydrofoil boat stability, lead to choosing to adapt the existing stability model developed for airplanes. The first part of this chapter is based on the 9^{th} chapter from the book "Flight Vehicle Aerodynamics" by Drela [12], which deals with flight dynamics. In this book Drela discusses the "airplane dynamic stability theory". The main difference between the dynamics for a hydrofoil boat and an airplane lies in the presence of the free water surface, above which the lift-generating surfaces do not generate any significant lift. Further in this chapter an article on the stability analysis of a hydrofoiling boat by Y. Masuyama [6] is discussed.

Both works, of Drela and Masuyama, are rooted in the same classical dynamic stability model which makes use of the equations of motion for a rigid body. These equations get linearized using small-disturbance theory. The book by Drela shows very clearly how the stability matrix is developed and helps to understand its different nuances. The article by Masuyama distinguishes itself by the various assumptions for the particular case of a hydrofoiling boat. His work also provides data to support these assumptions. Trough out this work differences between the approaches for airplanes and hydrofoil boats will be emphasized. Based on these works, an adapted model is derived for the specific case in this thesis.

3.1 Definitions and terminology

Hydrofoiling boats are a branch of maritime engineering which has a lot in common with aeronautics. This fact leads often to confusion in the used terminology. This section is put in place to have unambiguous terminology to avoid any confusion in the remainder of this thesis. The definitions and terminology of this section will be used unless stated otherwise.

3.1.1 Frames of reference

Mainly use maritime terminology will be used, as the subject of this thesis is a boat. The most important axis system will be an inertial, right-handed, earth-bound axis system with the Z-axis directed downwards, the X-axis parallel with the water-surface along the sailing direction of the boat and the Y-axis directed to starboard, perpendicular to the X and Z-axis. The second frame that is used, is a right-handed boat-fixed frame with the origin coinciding with the centre of gravity of the boat, the z-axis directed parallel to the LE of the Z-board and the x-axis along the symmetry line of the boat. Both frames can be found in Fig. 3.1: the earth-bound frame noted as X^e, Y^e, Z^e and the body-fixed frame noted as x^b, y^b, z^b.

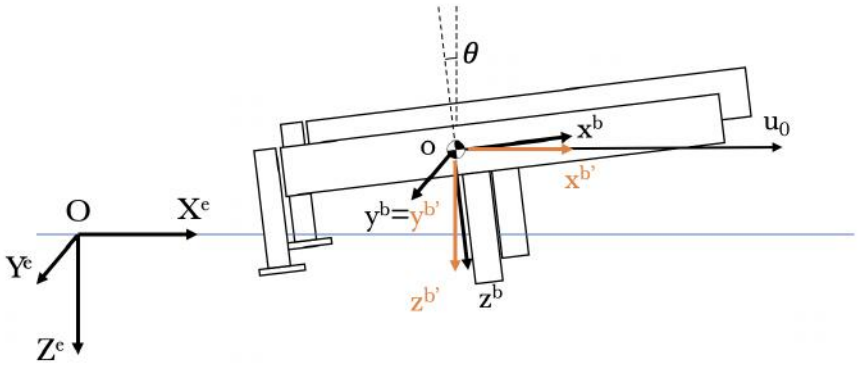

Figure 3.1: The earth-bound frame together with two options for the boat-fixed frame.

A third frame that will be used is the so-called *stability frame*. This frame is also a boat-fixed frame for which the origin is also coincident with the CoG. In equilibrium conditions the velocity vector will always lie in the xy-plane. This frame can be recognized as the orange axis-system in Fig. 3.1 noted with $x^{b'}, y^{b'}, z^{b'}$. In contrast to airplanes, for hydrofoil boats this stability frame always lies perpendicular to the water-surface as a hydrofoil boat in equilibrium conditions will remain at a fixed height above the water.

3.1.2 Components

The Viper is catamaran, this means that the boat features two parallel hulls. The two hulls are connected by the trampoline which is used as main operating area for the crew. As is usual in maritime terminology the right hull will be called the *starboard hull* and the left hull will be called the *port hull*. Each hull has two appendages: the main foil, which will from here on be called the *Z-board*, and the rudder. The rudder will be subdivided in the *rudder* (vertical part) and the *elevator* (horizontal part). The Viper has three sails: the *main sail*, the *jib* and the *gennaker*. The *mast* is the vertical structural component holding these sails in place. An overview of these most important parts if given in Fig. 3.2.

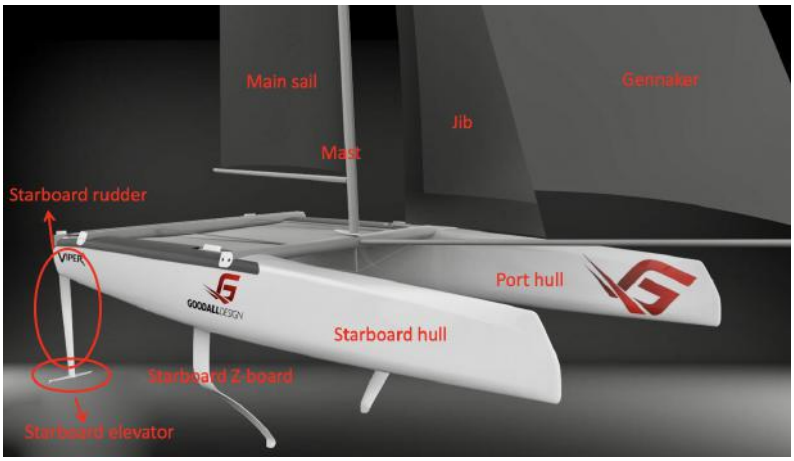

Figure 3.2: The earth-bound frame together with the boat-fixed frame.

3.1.3 Motions

In table 3.1 an overview of the terminology used for the various orientations, positions and motions can be found. The angles ϕ, θ and ψ are called the *Euler angles* and represent the orientation of the stability axes with respect to the Earth-bound frame. This Euler angles can be used to construct a transformation matrix, in which the order of the various rotation is of great importance. The emergence or immergence from the water is called the draft. As the Z-axis is directed downwards, a more positive draft means that boat lies deeper in the water. For accelerations the table can be extended by adding *acceleration* to the corresponding velocity. E.g. the angular acceleration around the Y-axis is called the *roll acceleration*. Fig. 3.3 gives a visual representation of these terms.

Table 3.1: An overview of the used terminology for the various motions.

	angle	**position**	**angular velocity**	**velocity**
X	ϕ (heel)	x (-)	p (pitch)	u (surge)
Y	θ (trim)	y (-)	q (roll)	v (sway)
Z	ψ (heading)	z (draft)	r (yaw)	w (heave)

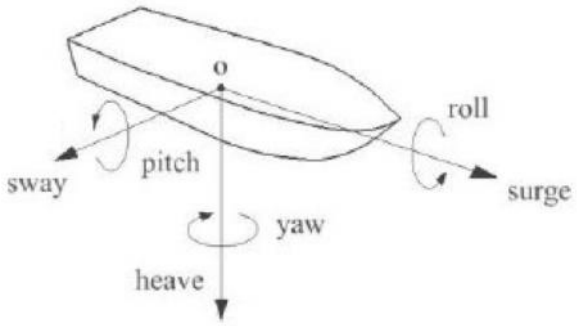

Figure 3.3: The various velocities visualized [4].

3.2 Airplane dynamic stability theory

Both because of the similarities between airplanes and hydrofoil boats and due to the fact that -in contrast with hydrofoil boats- the dynamic stability model of airplanes is well-documented, it is a logical starting point to develop a model for a hydrofoil boat. The following section is based on the book "Flight Vehicle Aerodynamics" by Drela [12]. This book clearly demonstrates how the stability matrix is developed and this procedure will be paraphrased here.

3.2.1 Definitions

The position of the earth-fixed frame can be chosen arbitrary. Here, the XY-plane of this frame is chosen parallel to the water surface as is displayed in Fig. 3.1. The motion and the position of the boat is defined with R^e_O, $U^{b'}$ and $\Omega^{b'}$. These are respectively the position vector of the CoG in the earth-bound frame and the velocity vector and rotation vector in the stability frame. These vectors together with the Euler angles allow us to construct a state vector $X(t)$ which defines both the instantaneous position and orientation and the motions of the boat. The state vector $X(t)$ contains position, orientation, velocity and angular velocity where the first two are defined in the earth-fixed frame and the last two in the stability frame. This gives us:

$$X(t) = \{x^e\ y^e\ z^e\ \phi\ \theta\ \psi\ u\ v\ w\ p\ q\ r\}^T \tag{3.1}$$

This state vector is a sequence of the position vector R_O^e (x^e, y^e, z^e), Euler angles (ϕ, θ, ψ), velocity vector $U^{b'}$ (u, v, w) and angular velocity vector $\Omega^{b'}$ (p, q, r). These 12 components determine the state of the boat completely. To solve these 12 components, 12 equations should be found. This is done trough 6 *kinematic relations* and 6 *dynamic relations*. The kinematic relations relate the earth-fixed frame to the body fixed frame both for the position rate and the orientation rate. The 6 dynamic relations are based on the linear and angular momentum equations (Newton's Second Law) and contain the forces and moments working on the boat.

The Euler angles allow us to construct a transformation matrix $\overline{\overline{T}}^e_{b'}$ from the stability to the earth-bound system. A similar matrix can be found for translation between the boat-fixed frame and earth bound frame. The transformation of the boat's velocity in the stability frame to the earth-fixed frame is done as followed:

$$U^e = \overline{\overline{T}}^e_{b'} U^{b'} \tag{3.2}$$

The transformation matrix $\overline{\overline{T}}^e_{b'}$ is formed from the product of three simple rotations in the standard sequence $-\phi$, $-\theta$, $-\psi$ respectively around $e_x^{b'}$, $e_y^{b'*}$ and $e_z^{b'**}$[13]. The axes, as by the time the second rotation is performed the axes of stability frame will already be changed. The notations C_x and S_x in Eq. 3.3 denote the cosine and sine of x.

$$\overline{\overline{T}}^e_b = \begin{bmatrix} C_\psi & -S_\psi & 0 \\ S_\psi & C_\psi & 0 \\ 0 & 0 & 1 \end{bmatrix} \begin{bmatrix} C_\theta & 0 & S_\theta \\ 0 & 1 & 0 \\ -S_\theta & 0 & C_\theta \end{bmatrix} \begin{bmatrix} 1 & 0 & 0 \\ 0 & C_\phi & -S_\phi \\ 0 & S_\phi & C_\phi \end{bmatrix} \tag{3.3}$$

The inverse transformation, from the earth-fixed frame to the stability frame, is composed of the rotation sequence ψ, θ, ϕ which results in the inverse matrix $\overline{\overline{T}}^b_e$.

3.2.2 Kinematic relations

Position rate

The position rate of the reference point R_O is equal to the body's velocity U^e in earth axes. This is described in Eq. 3.4.

$$\frac{d}{dt} R_O^e = U^e = \overline{\overline{T}}^e_b U^b \tag{3.4}$$

As the velocity is usually given in the body axes and the position in the earth axes, Eq. 3.4 is extended with the transformation matrix $\overline{\overline{T}}^e_b$. This is written in full in Eq. 3.5.

$$\frac{d}{dt} \begin{Bmatrix} x^e \\ y^e \\ z^e \end{Bmatrix} = \begin{bmatrix} C_\theta C_\psi & S_\phi S_\theta C_\psi - C_\phi S_\psi & C_\phi S_\theta C_\psi + S_\phi S_\psi \\ C_\theta S_\psi & S_\phi S_\theta S_\psi + C_\phi C_\psi & C_\phi S_\theta S_\psi + S_\phi C_\psi \\ -S_\theta & S_\phi C_\theta & C_\phi C_\theta \end{bmatrix} \begin{Bmatrix} u \\ v \\ w \end{Bmatrix} \tag{3.5}$$

By elaborating Eq. 3.5 the first 3 kinematic relations can easily be found.

Orientation rate

The rotation rate $\overrightarrow{\Omega}^e$ is composed of the three rotation rates respectively around x^e, y^e and z^e. $\overrightarrow{\Omega}^e$ can be related to the Euler angle rates via the following expression:

$$\begin{Bmatrix} \Omega_x^e \\ \Omega_y^e \\ \Omega_z^e \end{Bmatrix} = \left[\overline{\overline{K}}_b^e\right] \begin{Bmatrix} \dot{\phi} \\ \dot{\theta} \\ \dot{\psi} \end{Bmatrix} \tag{3.6}$$

where the matrix $\overline{\overline{K}}_b^e$ is the transformation matrix between the rotation rates and the Euler angle rates and has the from from Eq. 3.7. The exact derivation of this matrix is not included here as this would lead too far.

$$\overline{\overline{K_b^e}} = \begin{bmatrix} C_\psi C_\theta & -S_\psi & 0 \\ S_\psi C_\theta & C_\psi & 0 \\ -S_\theta & 0 & 1 \end{bmatrix} \tag{3.7}$$

When Eq. 3.6 gets premultiplied with the transformation matrix $\overline{\overline{T}}_e^b$ we arrive at the rotation rates around the body-fixed axes $\overrightarrow{\Omega}^b$.

$$\begin{Bmatrix} \Omega_x^b \\ \Omega_y^b \\ \Omega_z^b \end{Bmatrix} = \left[\overline{\overline{T}}_e^b\right] \begin{Bmatrix} \Omega_x^e \\ \Omega_y^e \\ \Omega_z^e \end{Bmatrix} = \left[\overline{\overline{T}}_e^b\right] \left[\overline{\overline{K}}_b^e\right] \begin{Bmatrix} \dot{\phi} \\ \dot{\theta} \\ \dot{\psi} \end{Bmatrix} \tag{3.8}$$

Inverting the expression gives us the rates of change of the Euler angles:

$$\frac{d}{dt} \begin{Bmatrix} \phi \\ \theta \\ \psi \end{Bmatrix} = \begin{bmatrix} 1 & S_\phi T_\theta & C_\phi T_\theta \\ 0 & C_\phi & -S_\phi \\ 0 & S_\phi / C_\theta & C_\phi / C_\theta \end{bmatrix} \begin{Bmatrix} \Omega_x^b \\ \Omega_y^b \\ \Omega_z^b \end{Bmatrix} \tag{3.9}$$

3.2.3 Dynamic relations

The linear momentum equation is usually expressed in the earth's inertial frame with the total force acting on the boat being a combination of the hydrodynamic force F^e and the gravitational force mg^e. This can be transformed to an equation where all components are expressed in the stability frame with the help of the transformation matrix $\overline{\overline{T}}_e^{b'}$. For the complete procedure we refer to Drela [12]. The result is given below:

$$F^{b'} + mg^{b'} = m(\dot{U}^{b'} + \Omega^{b'} \times U^{b'}) \tag{3.10}$$

$$\text{with: } F^{b'} = \begin{Bmatrix} X \\ Y \\ Z \end{Bmatrix}$$

The method to attain the angular momentum equation in the stability frame is very similar and is given by Eq. 3.11.

$$M^{b'} = \overline{\overline{I}}^{b'} \dot{\omega}^{b'} + \Omega^{b'} \times (\overline{\overline{I}}^{b'} \Omega^{b'}) \tag{3.11}$$

$$\text{with: } M^{b'} = \begin{Bmatrix} L \\ M \\ N \end{Bmatrix}$$

$\overline{\overline{I}}^{b'}$ the inertia tensor of the boat. The total forces and moments along or around the different axes of the stability frame are noted as X, Y and Z for the forces and L, M and N for the moments. The reason to express the equations above in the stability frame is mainly due to the fact that this results in less complicated formulas as the inertia tensor $\overline{\overline{I}}^{b}$ stays constant in this reference frame as the stability frame rotates together with the boat.

3.2.4 Equations of motion

Combining the kinematic relations with the dynamic relations now leads to 12 ODEs . There are 2 kinematic relations for both the position rate (Eq. 3.4) and orientation rate (Eq. 3.6) (for all 3 dimensions) which lead to the first 6 relations. The 2 dynamic relations (Eq. 3.10) (Eq. 3.11) (for all 3 dimensions) lead to the next 6 relations. This results in the system developed in Eq. 3.12-3.15.

$$\begin{aligned} \dot{x}^e &= C_\theta C_\psi u + (S_\phi S_\theta C_\psi - C_\phi S_\psi)v + (C_\phi S_\theta C_\psi + S_\phi S_\psi)w \\ \dot{y}^e &= C_\theta S_\psi u + (S_\phi S_\theta S_\psi + C_\phi C_\psi)v + (C_\phi S_\theta S_\psi + S_\phi C_\psi)w \\ \dot{z}^e &= -S_\theta u + S_\phi C_\theta v + C_\phi C_\theta w \end{aligned} \tag{3.12}$$

$$\begin{aligned} \dot{\phi} &= p + qS_\phi T_\theta + rC_\phi T_\theta \\ \dot{\theta} &= qC_\phi - rS_\phi \\ \dot{\psi} &= qS_\phi / C_\theta + rC_\phi / C_\theta \end{aligned} \tag{3.13}$$

$$\begin{aligned} X - mgS_\theta &= m(\dot{u} + qw - rv) \\ Y + mgS_\phi C_\theta &= m(\dot{v} + ru - pw) \\ Z + mgC_\phi C_\theta &= m(\dot{w} + pv - qu) \end{aligned} \tag{3.14}$$

$$\begin{aligned} L &= I_{xx}\dot{p} - I_{xy}\dot{q} - I_{xz}\dot{r} + (I_{zz} - I_{yy})qr - I_{yz}(q^2 - r^2) - I_{xz}pq + I_{xy}pr \\ M &= I_{yy}\dot{q} - I_{xy}\dot{p} - I_{yz}\dot{r} + (I_{xx} - I_{zz})rp - I_{xz}(r^2 - p^2) - I_{xy}qr + I_{yz}qp \\ N &= I_{zz}\dot{r} - I_{xz}\dot{p} - I_{yz}\dot{q} + (I_{yy} - I_{xx})pq - I_{xy}(p^2 - q^2) - I_{yz}qr + I_{xz}qp \end{aligned} \tag{3.15}$$

Multiplying Eq. 3.14 with $1/m$ and Eq. 3.15 with the inverse of the inertia tensor $\overline{\overline{I}}^{b'\,-1}$ allows to write these formulas in an explicit form for $\dot{u}$, $\dot{v}$, $\dot{w}$, $\dot{p}$, $\dot{q}$ and $\dot{r}$. Eq. 3.12-3.15 can now be

written in a general form with the help of the state vector $X(t)$ from Eq. 3.1 as is demonstrated in Eq. 3.16. The force $F^{b'}$ and moment $M^{b'}$ are unknown and will be linearized making use of small-disturbance theory.

$$\dot{X(t)} = f(X(t)) \tag{3.16}$$

3.2.5 Linearization

Assume an equilibrium state X_0. If the boat now experiences a small, arbitrary deviation from this state every term would get perturbed. This can be expressed by substituting every term by its equilibrium value (noted with subscript 0) plus a deviation from this equilibrium value (noted with Δ). This is demonstrated in Eq. 3.18 for first relation of Eq. 3.14.

$$X - mg\ sin(\theta) = m(\dot{u} + qw - rv) \tag{3.17}$$

$$\begin{aligned} \Leftrightarrow X_0 + \Delta X - mg\ sin(\theta_0 + \Delta\theta) = \\ m(\dot{u_0} + \Delta\dot{u} + (q_0 + \Delta q)(w_0 + \Delta w) - (r_0 + \Delta r)(v_0 + \Delta v) \end{aligned} \tag{3.18}$$

After substituting these perturbations in all 12 ODEs of Eq. 3.12-3.15, some simplifications can be made depending on the type of aircraft/boat under consideration (e.g. symmetric flight, symmetric boat, equilibrium values being zero, ...). The simplifications from Drela will not be discussed here in detail as they are not relevant for the case of a hydrofoil boat. They are summarized as:

$$w_0 = v_0 = p_0 = q_0 = r_0 = \dot{u}_0 = \dot{v}_0 = \dot{w}_0 = \dot{p}_0 = \dot{q}_0 = \dot{r}_0 = I_{xy} = I_{yz} = 0 \tag{3.19}$$

The total forces and moments depend on the entire flow regime around the boat. To make the expression above tractable, they are assumed to be a function of the state(-vector) of the boat and its derivatives. E.g. for the force along the Z-axis this becomes:

$$Z \rightarrow Z(X(t), \dot{X}(t)) = Z(u, \dot{u}, \ddot{u}, ..., q, \dot{q}, \ddot{q}, ...)$$

Forces and moment can now be approximated using a first-order Taylor expansion around the equilibrium state. Depending on the case under consideration, certain terms are or are not taken into account. This will be discussed later. The Taylor expansion is demonstrated in Eq. 3.20 for the longitudinal vertical force Z with a_i a general representation for a state-vector component.

$$\Delta Z = \sum_i \frac{\delta Z}{\delta a_i}\Delta a_i = \frac{\delta Z}{\delta u}\Delta u + \frac{\delta Z}{\delta w}\Delta w + \frac{\delta Z}{\delta q}\Delta q + \frac{\delta Z}{\delta \theta}\Delta\theta + ... \tag{3.20}$$

3.2.6 Stability matrix

With the help of the state-vector, the system of Eq. 3.12-3.15 can be written in a more convenient matrix notation.

$$\frac{d}{dt}\left[\begin{array}{c} \Delta u \\ \Delta w \\ \Delta q \\ \Delta\theta \\ \hline \Delta v \\ \Delta p \\ \Delta r \\ \Delta\phi \\ \hline \Delta x^e \\ \Delta y^e \\ \Delta z^e \\ \Delta\psi \end{array}\right] = \left[\begin{array}{cccc|cccc|c} . & . & . & . & * & * & * & * & * \\ . & . & . & . & * & * & * & * & * \\ . & . & . & . & * & * & * & * & * \\ . & . & . & . & * & * & * & * & * \\ \hline * & * & * & * & . & . & . & . & * \\ * & * & * & * & . & . & . & . & * \\ * & * & * & * & . & . & . & . & * \\ * & * & * & * & . & . & . & . & * \\ \hline . & . & . & . & . & . & . & . & \\ . & . & . & . & . & . & . & . & \\ . & . & . & . & . & . & . & . & \\ . & . & . & . & . & . & . & . & \end{array}\right] \left[\begin{array}{c} \Delta u \\ \Delta w \\ \Delta q \\ \Delta\theta \\ \hline \Delta v \\ \Delta p \\ \Delta r \\ \Delta\phi \\ \hline \Delta x^e \\ \Delta y^e \\ \Delta z^e \\ \Delta\psi \end{array}\right] \tag{3.21}$$

The resulting matrix is called the stability matrix, A. The elements denoted with "$\cdot$" are the non zero-elements in this matrix when the simplifications applicable for airplanes are implemented[1]. The eigenmodes and eigenvalues of this matrix allow to find the natural response of this system, which is a superposition of the eigenmodes. The eigenvectors will determine if a certain mode is stable or not.

The stability matrix is characterized by three distinct subsets: the first four rows form the *longitudinal subset*, the next four rows forming the *lateral subset* and the last four rows forming the *navigation subset*. A useful property for airplanes is that the three kinds of motions (longitudinal, lateral and navigational) can be treated separately as the block-matrices are decoupled, due to the zero-blocks. However, for hydrofoil boats, this decoupling characteristic is no longer valid as non-zero terms appear in the blocks that were previously zero. This has various reasons: (1) the aerodynamic forces of the sail will simultaneously affect longitudinal and lateral motions. E.g. if the boatspeed increases (longitudinal motion) the sail will produce less lift (lateral force) and consequently will experience less heel. (2) The forces and moments will have a dependency on the draft z, where as this is clearly not the case for airplanes. The terms denoted with $*$ in the stability matrix above are then also non-zero terms.

[1] As was mentioned before, the simplifications for an airplane are not discussed in detail as they are not relevant for the case of a hydrofoil boat. They are here assumed tacitly to obtain the regular stability matrix form.

3.3 Model by Masuyama

Already in 1987, well before the big development rush we are seeing today in the field of hydrofoils, Y. Masuyama pioneered a dynamic stability theory specifically for hydrofoil boats [6]. His theory is based on the same model as the "airplane dynamic stability theory" of previous section, it distinguishes itself by the made assumptions. In this section his paper on this stability analysis is discussed. The work of Masuyama is very similar to that of Drela but is more compact as it does not take into account every possible motion as Drela does.

3.3.1 Equations of motion

The model of Masuyama is based on the same 6 dynamic equations of Eq. 3.14-3.15 in the non-inertial body-fixed stability frame. This frame is non-inertial as it not only translate but also rotates in reference to the earth-bound frame. Again, a small deviation from an equilibrium state will be assumed and the equations will be linearized as in sec. 3.2.5. Every term gets substituted for its equilibrium value plus a deviation from this equilibrium state. As was mentioned in sec. 3.2.6 a perturbation of any form will simultaneously affect longitudinal and lateral motions, which is why the 6 equations will need to be solved simultaneously. Many terms will disappear as some components of the equilibrium state vector X_0 will be zero. The equilibrium values for vertical velocity component w_0 and for the trim angle θ_0 will be zero because of the use of stability axes[2]. For these stability axes the velocity vector, in equilibrium conditions, will always lie in the XY-plane. Consequently this vector will always be horizontal as a hydrofoil boat in equilibrium conditions has a constant draft. Due to the symmetry of the boat, the moment of inertia I_{xy} and I_{yz} will also be zero. Rotational rates will also be zero as no turning is assumed. To summarize:

$$w_0 = \theta_0 = p_0 = q_0 = r_0 = \dot{u}_0 = \dot{v}_0 = \dot{w}_0 = \dot{p}_0 = \dot{q}_0 = \dot{r}_0 = I_{xy} = I_{yz} = 0 \tag{3.22}$$

The experienced angle deviations in trim and heel will be relatively small and their cosines and sines can thus be approximated linearly ($cos(x) \approx 1$; $sin(x) \approx x$). The resulting sines and cosines are further elaborated with the trigonometric relations for angle sums. Furthermore, the second order effects are also negligibly small. This gets demonstrated for the linear momentum equation in the Y-direction in Eq. 3.23.

$$\begin{aligned}
& Y + mgS_\phi C_\theta = m(\dot{v} + ru - pw) \\
\Rightarrow\quad & Y_0 + \Delta Y + mg\ sin(\phi_0 + \Delta\phi)cos(\Delta\theta) \simeq m(\Delta\dot{v} + (\Delta r)(u_0 + \Delta u) - (\Delta p)(\Delta w)) \\
\Rightarrow\quad & Y_0 + \Delta Y + mg\ (sin(\phi_0) \cdot 1 + cos(\phi_0) \cdot \Delta\phi) \cdot 1 \simeq m(\Delta\dot{v} + \Delta r \cdot u_0) \\
\Rightarrow\quad & \Delta Y + mg\ cos(\phi_0) \cdot \Delta\phi \simeq m(\Delta\dot{v} + \Delta r \cdot u_0)
\end{aligned} \tag{3.23}$$

[2]Their deviation terms Δw and $\Delta\theta$ are not zero. This is due to the fact that just like a regular body-fixed frame, the stability axes rotate together with the boat.

The complete system then reduces to Eq. 3.24.

$$\begin{cases} \Delta X - mg\Delta\theta \simeq m(\Delta\dot{u} - \Delta r \cdot v_0) \\ \Delta Y + mg\Delta\phi \simeq m(\Delta\dot{v} + \Delta r \cdot u_0) \\ \Delta Z - mg\phi_0\Delta\phi \simeq m(\Delta\dot{w} + \Delta p \cdot v_0 - \Delta q \cdot u_0) \\ \Delta L \simeq I_{xx}\Delta\dot{p} - I_{xz}\Delta\dot{r} \\ \Delta M \simeq I_{yy}\Delta\dot{q} \\ \Delta N \simeq I_{zz}\Delta\dot{r} - I_{zx}\Delta\dot{p} \end{cases} \tag{3.24}$$

The motions around the Z-axis are not assumed by Masuyama. He mentions that this motion does not affect the dynamic stability analysis. However, as he mentioned himself, decoupling of the various motions is not guaranteed, meaning ψ, r and $\dot{r}$ will surely have an influence on the dynamical behaviour of the boat. This assumption is not supported properly in his paper. Nevertheless, in this section his reasoning will be followed. As motions around the Z-axis are omitted, the 6^{th} relation in Eq. 3.24 will disappear together with all the $\dot{r}$, r and ψ components. This would lead to only 5 equations, and the system contains, after linearization of the forces and moments, 6 unknowns: u, v, w, ϕ, θ, z. An extra equation comes from the kinematic relation linking the draft z with the heave motion w.

$$\begin{cases} \Delta X - mg\Delta\theta = m(\Delta\dot{u}) \\ \Delta Y + mg\Delta\phi = m(\Delta\dot{v}) \\ \Delta Z + mg\phi_0\Delta\phi = m(\Delta\dot{w} + \Delta p \cdot v_0 - \Delta q \cdot u_0) \\ \Delta L = I_{xx}\Delta\dot{p} \\ \Delta M = I_{yy}\Delta\dot{q} \\ \Delta\dot{z} = \Delta w - u_0\Delta\theta + v_0\Delta\phi \end{cases} \tag{3.25}$$

Two more kinematic equations are implied tacitly by Masuyama: $\dot{\theta} \approx q$ and $\dot{\phi} \approx p$. These relations are however only accurate if the angle of heel in equilibrium ϕ_0 is of the same order of the perturbations ($\phi_0 \sim \Delta\theta$). For the case that will be considered in this thesis, the angle of heel is assumed to be zero as the boat is most efficient when sailed "flat". If a substantial angle of heel needs to be included, the system should be completed with all three relations from Eq. 3.13. Masuyama states that for his equilibrium, the boat has a heel angle which was smaller than 5° [5][3] meaning that the above assumption is justified.

3.3.2 Linearization

The forces and moments are again linearized by assuming them as a function of the various kinematic parameters and expanding them using a first-order Taylor expansion. This is demonstrated

[3]This was translated from his Japanese paper.

for the force in the X-direction in Eq. 3.26. The same can be done for ΔY, ΔZ, ΔL and ΔM.

$$\begin{aligned}\Delta X = \sum_i \frac{\delta X}{\delta a_i}\Delta a_i = X_u\Delta u + X_{\dot{v}}\Delta\dot{v} + X_w\Delta w + X_{\dot{w}}\Delta\dot{w} + \\ X_\phi\Delta\phi + X_p\Delta\dot{\phi} + X_{\dot{p}}\Delta\ddot{\phi} + X_\theta\Delta\theta + X_q\Delta\dot{\theta} + X_{\dot{q}}\Delta\ddot{\theta} + X_z\Delta z\end{aligned} \tag{3.26}$$

With $X_a = \frac{\delta X}{\delta a}$ and similar for the other terms.

The first equation of Eq. 3.25 then becomes the following linear equation:

$$\begin{aligned}m\Delta\dot{u} + mg\Delta\theta - X_u\Delta u + X_{\dot{v}}\Delta\dot{v} + X_w w + X_{\dot{w}}\Delta\dot{w} + \\ X_\phi\Delta\phi + X_p\Delta\dot{\phi} + X_{\dot{p}}\Delta\ddot{\phi} + X_\theta\Delta\theta + X_q\Delta\dot{\theta} + X_{\dot{q}}\Delta\ddot{\theta} + X_z\Delta z = 0\end{aligned} \tag{3.27}$$

This can be done for all six expressions in Eq. 3.25. Since this leads to a system of six linear ODEs their solutions can be written as:

$$\begin{aligned}\Delta u = u_1 e^{\lambda t}\ ,\ \Delta v = v_1 e^{\lambda t}\ ,\ \Delta w = w_1 e^{\lambda t}\ , \\ \Delta\phi = \phi_1 e^{\lambda t}\ ,\ \Delta\theta = \theta_1 e^{\lambda t}\ ,\ \Delta z = z_1 e^{\lambda t}\ .\end{aligned} \tag{3.28}$$

Which, after substituting this solution in formula (4.22), leads to the following expression (which again is similar for all 6 equations of the system):

$$\begin{aligned}(m\lambda - X_u)u_1 - (X_{\dot{v}}\lambda + X_v)v_1 - (X_{\dot{w}}\lambda + X_w)w_1 \\ -(X_{\dot{p}}\lambda^2 + X_p\lambda + X_\phi)\phi_1 - (X_{\dot{q}}\lambda^2 + X_q\lambda + X_\theta - mg)\theta_1 - X_z z_1 = 0\end{aligned} \tag{3.29}$$

3.3.3 Stability Matrix

If the above procedure is performed for all six equations in the system of Eq. 3.25, the ODE-system can be rewritten in a matrix notation. Setting the determinant of the resulting matrix to zero leads to the eigenvalues of this system.

$$\begin{bmatrix} m\lambda - X_u & -X_{\dot{v}}\lambda - X_v & -X_{\dot{w}}\lambda - X_w & -X_{\dot{p}}\lambda^2 - X_p\lambda - X_\phi & -X_{\dot{q}}\lambda^2 - X_q\lambda - X_\theta + mg & -X_z \\ -Y_u & (m - Y_{\dot{v}})\lambda - Y_v & -Y_{\dot{w}}\lambda - Y_w & -Y_{\dot{p}}\lambda^2 - Y_p\lambda - (mg + Y_\phi) & -Y_{\dot{q}}\lambda^2 - Y_q\lambda - Y_\theta & -Y_z \\ -Z_u & -Z_{\dot{v}}\lambda - Z_v & (m - Z_{\dot{w}})\lambda - Z_w & -Z_{\dot{p}}\lambda^2 + (mv_0 - Z_p)\lambda - Z_\phi) & -Z_{\dot{q}}\lambda^2 - (mu_0 + Z_q)\lambda - Z_\theta & -Y_z \\ -L_u & -L_{\dot{v}}\lambda - L_v & -L_{\dot{w}}\lambda - L_w & (I_{xx} - L_{\dot{p}})\lambda^2 - L_p\lambda - L_\phi) & -L_{\dot{q}}\lambda^2 - L_q\lambda - L_\theta & -L_z \\ -M_u & -M_{\dot{v}}\lambda - M_v & -M_{\dot{w}}\lambda - M_w & -M_{\dot{p}}\lambda^2 - M_p\lambda - M_\phi) & (I_{yy} - M_{\dot{q}})\lambda^2 - M_q\lambda - M_\theta & -M_z \\ 0 & 0 & -1 & -v_0 & u_0 & \lambda \end{bmatrix} \begin{bmatrix} u_1 \\ v_1 \\ w_1 \\ \phi_1 \\ \theta_1 \\ z \end{bmatrix} = 0 \tag{3.30}$$

The resulting square matrix is again a stability matrix A. By solving the characteristic equation the eigenvalues can be determined and consequently would lead to the eigenvectors.

$$\begin{aligned}|A - \lambda I| &= 0 \\ &= f_8\lambda^8 + f_7\lambda^7 + f_6\lambda^6 + f_5\lambda^5 + f_4\lambda^4 + f_3\lambda^3 + f_2\lambda^2 + f_1\lambda + f_0\end{aligned} \tag{3.31}$$

The reason there are 8 and not 6 eigenvalues is due to the two tacitly implied equations mentioned earlier for the Euler angle rates. There are in fact 8 ODEs, if you include $\dot{\phi} \approx p$ and $\dot{\theta} \approx q$.

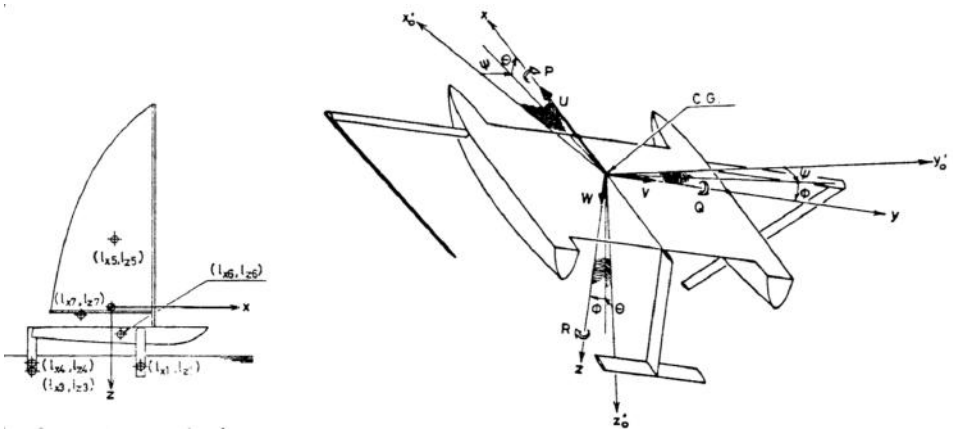

Figure 3.4: The setup used in Masuyama's paper [5].

3.3.4 Stability derivatives

To solve the characteristic equation of the previous section, numeric values are needed for the different derivatives. The derivatives can be determined separately for the different components of the boat. These components are the two Z-boards, the two elevators, the two rudders and the sails as a whole. Masuyama [6] provides a method on how to calculate the derivatives for all these components assuming the drag and lift coefficients are known. His method is valid the case of a simple dihedral foil setup for which the geometry of the foils can be expressed easily in function of a limited amount of parameters. This setup is shown in Fig. 3.4, the starboard foil is submerged for 0.3 m and the port foil for 0.79 m. For the case of the Viper this would to too many simplifications as the geometry is much more complicated. Also, both the C_L and C_D curves need to be known for all the parameters in the state-vector to follow Masuyama's procedure. His procedure will not be discussed here in detail as the derivatives in this work will be calculated using CFD .

Masuyama's work provides numerical values for all these derivatives. The setup of the Viper and the boat studied in the work of Masuyama differ a lot, but the values provided can still be of use to get a better understanding of the different behaviours as the principles are still in tact. All the numerical values are collected in appendix 7.2. The last column with the dimensionless values was added to get a better idea of the relative importance of the different derivatives.

A first aspect which can be observed is that the derivatives with respect to (angular) accelerations ($\dot{v}$, $\dot{w}$, $\dot{p}$ and $\dot{q}$) are negligibly small.

If the dimensionless derivatives are sorted for their absolute value other effects can be seen as well. The 14 largest derivatives are collected in Table 3.2, of a total of 60 derivatives. It was demonstrated before that the decoupling of longitudinal motions from the lateral motions

is not possible for a hydrofoil boat. Still, it can be seen in Table 3.2, that the derivatives of a symmetric force or moment to a symmetric motion or rotation will have a larger absolute value than its derivatives to a asymmetric motion or rotation and vice versa. For some derivatives this is not the case. (E.g. L_{zi}.) This can be accounted to the asymmetric setup of the boat (see sec. 3.3.4). If the boat would be setup symmetrically, equal but opposite terms are expected for the individual derivatives of the two foils. These terms are set in bold in table 3.2. For these large derivatives it can be seen that the decoupling is exclusively due to the difference between port and starboard foil: as the port foil is submerged more it will have larger derivatives.

The coupling effect of the sail is more of an influence on the smaller derivatives which are not included in the sorted table but can be seen in appendix 7.2. It can be noted how the sail has a larger influence in the case of lateral motions (p and v). The lateral motions will be coupled more strongly to longitudinal motions than the other way around.

It can be concluded that the coupling effects will be a lot smaller if a symmetric setup is assumed where both foils are equally submerged. If simultaneously, only longitudinal motions are assumed the coupling effect will become negligible. The assumption of a symmetric setup is justified by the fact that the boat is most efficient when it is sailed flat without any heel. If only the longitudinal forces and moments and their longitudinal derivatives are taken into account, the influence of the sail becomes small. This will be the argument to consider only longitudinal motions with longitudinal forces and moments for a symmetric setup.

Table 3.2: The derivatives sorted for the absolute value of the dimensionless total derivative [6].

	j	st (i=1)	port (i=2)	elevator (i=3)	rudder (i=4)	sail (i=5)	total	dimensionless	absolute value
M_{ji}	w	31	181	-1198	0	0	-986	-3.590	3.59
L_{ji}	ϕ	-518	-2022	0	0	0	-2540	-2.905	2.91
Z_{ji}	w	-37.9	-212.7	-515.9	0	0	-766.5	-2.791	2.79
M_{ji}	q	-19	-100	-2800	-4	-34	-2957	-2.153	2.15
Y_{ji}	ϕ	-505	-1172	0	0	0	-1677	-1.918	1.92
Z_{ji}	z	-288	-605	-29	0	0	-922	-1.678	1.68
L_{ji}	**z**	**-250**	**890**	**0**	**0**	**0**	**640**	**1.165**	**1.16**
Y_{ji}	v	-26.7	-149.7	0	-56.7	-41.9	-275	-1.001	1.00
Y_{ji}	**z**	**-241**	**508**	**0**	**258**	**0**	**525**	**0.956**	**0.956**
Z_{ji}	ϕ	**-601**	**1397**	**0**	**0**	**0**	**796**	**0.910**	**0.910**
M_{ji}	z	139	401	-67	0	0	473	0.861	0.861
Z_{ji}	q	16	97	-1199	0	0	-1086	-0.791	0.791
Z_{ji}	θ	233	490	-67	0	0	656	0.750	0.750
M_{ji}	ϕ	**300**	**-936**	**0**	**0**	**0**	**-636**	**-0.727**	**0.727**

3.3.5 Stability

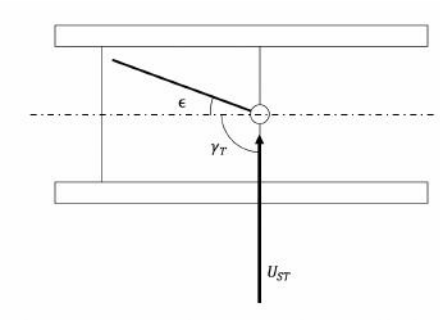

Figure 3.5: An overview of the used symbols in the paper by Masuyama.

The paper by Masuyama also contains three root locus diagrams for the model described above. These three diagrams are displayed in fig. 3.6 There are three possible wind-speeds U_{ST} and three possible setups of the sail, ϵ. They are all for a wind angle γ_T of 90°. These symbols can be seen in Fig. 3.5. The angle defining the sail setup ϵ is the angle the bottom of the sail makes with the centre-line of the boat. The smaller this angle is, the faster the boat will be going as it allows for an apparent wind[4] which comes more from the front. Some interesting conclusions come from his analysis. For decreasing ϵ , so increasing boatspeed, the boat becomes unstable. For every geometry and setup there is a maximal critical speed above which the boat becomes unstable. Above this critical speed, there still exist equilibrium state. Nevertheless, these equilibrium state will be dynamically unstable: a small perturbation would cause the boat to diverge from its equilibrium state. Without a stability analysis there can consequently be an over-estimation of the maximum attainable boat speed. This is visualised in fig. 3.7 with the help of a polar plot. In this kind of polar plot the angle represents the angle of the boat relative to the wind and the distance to the origin represents the speed. The over-estimation of the boatspeed is displayed by the gray area. This area represents the area where equilibria exist, but which are dynamically unstable. This clearly shows the importance of stability analysis to predict the behaviour of a boat.

[4]A boat experiences a *true wind*, which is the wind that would be felt when standing still, and a *headwind*, which is generated by its own speed. Combining the vectors of the true wind and headwind results in an apparent wind. If the speed increases, the headwind increases, and consequently the apparent wind will shift to the front.

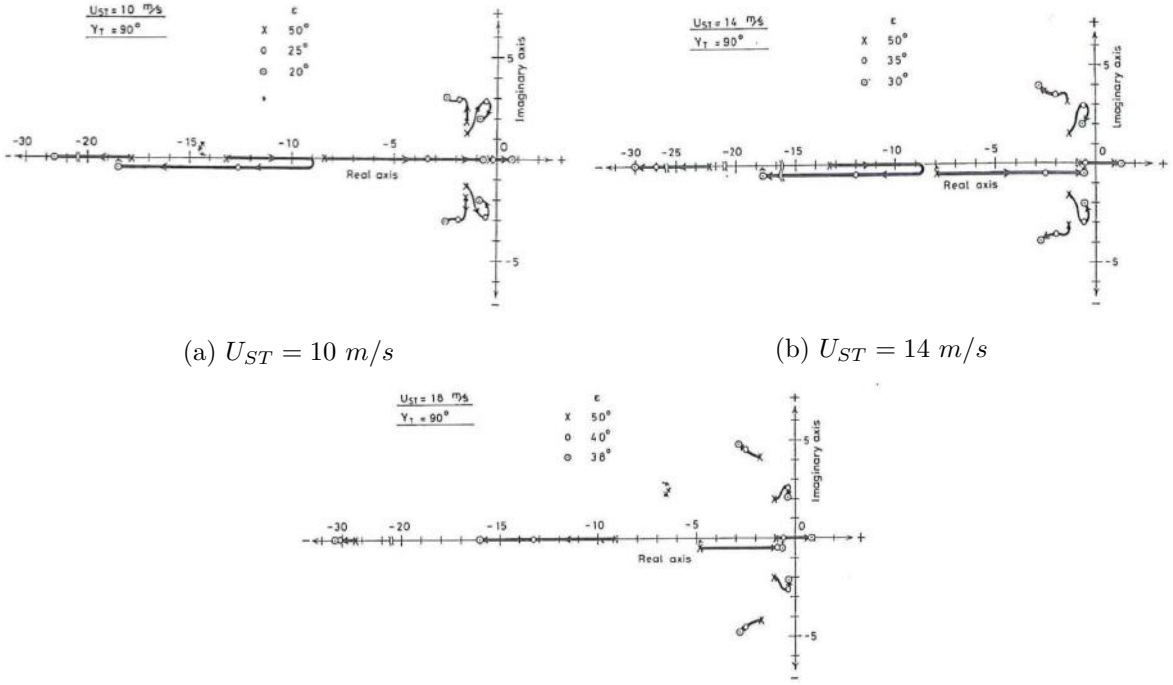

(a) $U_{ST} = 10\ m/s$

(b) $U_{ST} = 14\ m/s$

(c) $U_{ST} = 18\ m/s$

Figure 3.6: Root locus diagram for three different wind-speeds U_{ST} with varying sail setup ϵ [6].

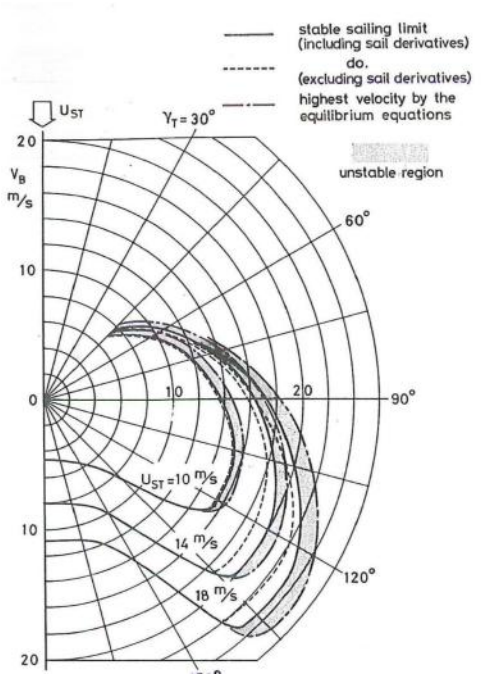

Figure 3.7: A polar plot of the maximum attainable velocity [6].

4

Longitudinal Stability Model

Certain simplifications can, and need to be made. These are based on the previous chapter. The intended results should somewhat justify the used resources. A two-phase simulation, where the whole boat and the free surface is included, would lead to more accurate results but would also lead to an unreasonably large mesh and simulation time. That is why it was chosen to only model the rudder, the elevator and the Z-board below the water surface and to assume all forces and moments above the water surface to be constant. In physical reality this would however not be true. The biggest contribution above the water originates from the sail. This immediately leads to another simplification: only *longitudinal* motions, rotations, forces and moments are taken into account. It can be seen from the data presented by Masuyama that *lateral* motions are more affected by the sail. Combining this with the fact that the sail is modelled as a constant force and moment, the results for the lateral motions won't have any value. Furthermore, rotations around the z-axis are more of interest for a directional stability analysis and will also be left out of the model. The approximation that all forces and moments above the water surface are constant is in the case of longitudinal motion justified: changing the draft or the trim angle barely influences the aerodynamic force . A surge disturbance Δu will be small compared to the equilibrium value u_0, and consequently also will have a limited effect on the aerodynamic force and moment.

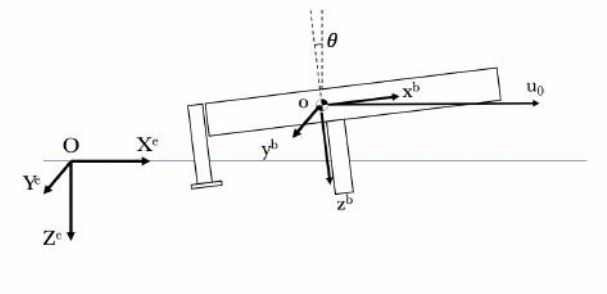

Figure 4.1: The earth-bound frame together with the boat-fixed frame.

4.1 Linearization

Based on the mentioned assumptions only 3 dynamic relations are included in the model: two force balances along the X- and Z-axis and one moment balance around the Y-axis. As this system only assumes one rotation where the models of Masuyama and Drela assumed two or three, the body-fixed frame is no longer the most convenient. The inertial earth-bound frame, displayed in Fig. 4.1 as the frame denoted with the uppercase $X^eY^eZ^e$, will lead to simpler equations. The moment of inertia I_{yy} and the moment M are defined around the centre of mass. Similar to the approaches in Ch. 3, the system will be assumed to be in equilibrium when it experiences a small, arbitrary perturbation. Every term then gets disturbed and can be replaced by its equilibrium value (noted with subscript 0) plus a deviation from this equilibrium value (noted with Δ). This procedure is written out in Eq. 4.1. The equilibrium values of the accelerations are of course zero. Furthermore are the equilibrium values of the forces and moments also zero, as this is the main premise to have an equilibrium. The 3 dynamic equations of this system are completed by two kinematic relations: one which couples the draft to the

vertical speed and one which couples the trim angle to the pitch velocity.

$$\begin{cases} X = m\dot{u} \\ Z + mg = m\dot{w} \\ M = I_{yy}\dot{q} \\ \dot{z} = -S_\theta u + S_\phi C_\theta v + C_\phi C_\theta w \\ \dot{\theta} = qC_\phi - rS_\phi \end{cases}$$

$$\Leftrightarrow \begin{cases} \Delta\dot{u} = \dfrac{\Delta X(u,z,\theta)}{m} \\ \Delta\dot{w} = \dfrac{\Delta Z(u,z,\theta)}{m} \\ \Delta\dot{q} = \dfrac{\Delta M(u,z,\theta)}{I_{yy}} \\ \Delta\dot{z} = \Delta w \\ \Delta\dot{\theta} = \Delta q \end{cases} \tag{4.1}$$

The resulting system differs much from e.g. the system by Masuyama in Eq. 3.25. The absence of gravity terms is due the choice for the inertial earth-bound frame where the gravity will always lie along the Z-axis even if the boat has a different trim angle. This was not the case for the boat-fixed frame. Also because of the use of this earth-bound frame the mixed terms (linear and angular velocity) are missing.

The only thing left to complete the procedure is linearizing the force and moment disturbance. Just like in the previous chapter the forces and moment are approximated by a Taylor expansion. This is made possible by assuming them to be a function of the kinematic parameters. Initially only the derivatives to the surge u, the draft z and the trim angle θ are considered. The derivatives to the vertical velocity w and the pitch q are much harder to calculate using CFD as they require transient simulations. This initial linearization is displayed in Eq. 4.2.

$$\Delta X = \sum_{i=1}^{3} \frac{\partial X}{\partial a_i}\Delta a_i = \frac{\partial X}{\partial u}\Delta u + \frac{\partial X}{\partial z}\Delta z + \frac{\partial X}{\partial \theta}\Delta\theta + 0 + 0 \tag{4.2}$$

This linearized system can be written in a matrix notation with a state-vector $X(t)$ and a stability matrix A, this is demonstrated in Eq. 4.3 and Eq. 4.4.

$$\frac{d}{dt}\begin{bmatrix} \Delta u \\ \Delta z \\ \Delta\theta \\ \Delta\dot{z} \\ \Delta\dot{\theta} \end{bmatrix} = [A] \cdot \begin{bmatrix} \Delta u \\ \Delta z \\ \Delta\theta \\ \Delta\dot{z} \\ \Delta\dot{\theta} \end{bmatrix} \tag{4.3}$$

$$[A] = \begin{bmatrix} \frac{1}{m}\frac{\partial X}{\partial u} & \frac{1}{m}\frac{\partial X}{\partial z} & \frac{1}{m}\frac{\partial X}{\partial \theta} & 0 & 0 \\ 0 & 0 & 0 & 1 & 0 \\ 0 & 0 & 0 & 0 & 1 \\ \frac{1}{m}\frac{\partial Z}{\partial u} & \frac{1}{m}\frac{\partial Z}{\partial z} & \frac{1}{m}\frac{\partial Z}{\partial \theta} & 0^* & 0^{**} \\ \frac{1}{I_{yy}}\frac{\partial M}{\partial u} & \frac{1}{I_{yy}}\frac{\partial M}{\partial z} & \frac{1}{I_{yy}}\frac{\partial M}{\partial \theta} & 0^* & 0^{**} \end{bmatrix} \tag{4.4}$$

4.2 Stability Derivatives

In sec. 3.3.4 it is demonstrated, based on the data by Masuyama, how decoupling of longitudinal and lateral motions can be justified if a symmetric boat is assumed with a zero heel angle. It is also justified to assume the aerodynamic forces and moments originating from the sail as constant in the case of longitudinal motion. If table 3.2 is now repeated but without the coupling and lateral terms, table 4.1 is found. This table contains the 10 largest dimensionless derivatives in absolute value. The first thing which can be seen in this table, is that the contribution of the sail is indeed exceptionally small for longitudinal motions as it has no contribution in all but one derivative. This justifies the constant aerodynamic forces and moments. The derivatives highlight in bold are, for now, assumed to be zero in the stability matrix A of Eq. 4.4. This shows that this stability matrix is far from accurate and these derivatives should be calculated or at least approximated.

It can be seen from table 4.1 that the elevator has large derivatives to the pitch velocity q. This can be explained as follows: a pitch velocity around the CoG is seen as a linear velocity $\overline{v} = \overline{q} \times r$ with q this pitch velocity and r the distance to the CoG . As the elevator is located far from the CoG v will be large, so that the elevator has large derivatives to the pitch velocity. A similar reasoning can be followed to explain why the elevator has a big contribution to the moment derivatives, M_{ji}.

Table 4.1: The derivatives as provided by Masuyama sorted for the absolute value of the dimensionless total derivative without coupling terms and lateral terms[6].

	j	st. (i=1)	port (i=2)	elevator (i=3)	rudder (i=4)	sail (i=5)	total	dimensionless	absolute value
M_{ji}	**w**	**31**	**181**	**-1198**	**0**	**0**	**-986**	**-3.590**	**3.59**
Z_{ji}	**w**	**-37.9**	**-212.7**	**-515.9**	**0**	**0**	**-766.5**	**-2.791**	**2.79**
M_{ji}	**q**	**-19**	**-100**	**-2800**	**-4**	**-34**	**-2957**	**-2.153**	**2.15**
Z_{ji}	z	-288	-605	-29	0	0	-922	-1.678	1.68
M_{ji}	z	139	401	-67	0	0	473	0.861	0.861
Z_{ji}	**q**	**16**	**97**	**-1199**	**0**	**0**	**-1086**	**-0.791**	**0.791**
Z_{ji}	θ	233	490	-67	0	0	656	0.750	0.750
M_{ji}	θ	-113	-325	-155	0	0	-593	-0.678	0.678
L_{ji}	θ	203	-721	0	0	0	-518	-0.592	0.592
X_{ji}	z	-52	-60	0	-35.2	0	-147.2	-0.268	0.268

Calculating the missing derivatives directly requires time-consuming transient simulations. For

the derivative to the pitch velocity the boat should be simulated to have a small pitch velocity, $q \neq 0$. The forces should be read at the moment the boat passes its equilibrium value. This transient simulation should however be long enough to make sure the flow has settled in a regime state. The derivative to heave can be calculated in a similar fashion. An approach for estimating these derivatives is proposed. By using the 9 derivatives which were already calculated in the stability matrix of Eq. 4.4, the other 6 derivatives can be approximated.

4.3 Approximations

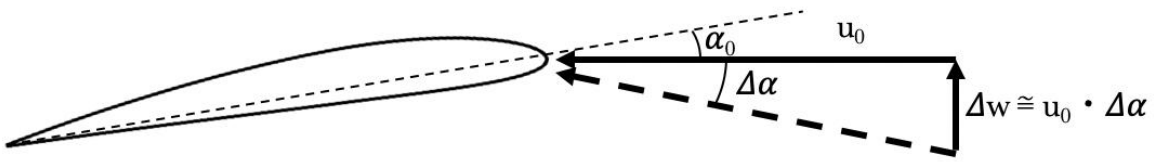

Figure 4.2: Effect of the vertical velocity, w.

The terms denoted with (*) in Eq. 4.4 are the force and moment derivatives to the speed in the vertical direction (heave), $\frac{\partial X}{\partial w}$,$\frac{\partial Z}{\partial w}$ and $\frac{\partial M}{\partial w}$. These terms will be approximated using the derivatives to the trim angle θ: $\frac{\partial X}{\partial \theta}$, $\frac{\partial Z}{\partial \theta}$ and $\frac{\partial M}{\partial \theta}$. As can be seen from Fig. 4.2 a perturbation Δw of the vertical velocity causes a change in angle of attack (AoA) α from the viewpoint of the foils. Since a hydrofoil boat sailing in equilibrium conditions will always have a horizontal speed, a change in AoA α is similar to a change in trim angle θ. A change in trim angle $\Delta\theta$ is seen by the foils as a change in AoA $\Delta\alpha$. The difference between changing the AoA and changing the trim angle lies in the fact that the submerged area will be different. Changing the AoA means that the same foil is used, but with different angle for the velocity vector. Changing the trim of the boat would not only lead to a change in AoA, but would also lead to a different foil geometry as the submerged areas will be different. These effects are situated at the free surface. It will be the area of the rudder which is most affected by this, but as the rudder will have barely no influence on the longitudinal stability these effects will be small and can be neglected, i.e. $\frac{\partial ...}{\partial \theta} \sim \frac{\partial ...}{\partial \alpha}$. Assuming small disturbances around an equilibrium point, $\frac{\partial Z}{\partial w}$ can be approximated as is shown in Eq. 4.5. The procedure for $\frac{\partial X}{\partial w}$ $\frac{\partial M}{\partial w}$ is analogous.

$$\frac{\partial Z}{\partial w} = \frac{\partial Z}{\partial \theta}\frac{\partial \theta}{\partial w} = \frac{\partial Z}{\partial \theta}\frac{\partial \alpha}{\partial w} \approx \frac{1}{u_0}\frac{\partial Z}{\partial \theta} \tag{4.5}$$

$$\text{with} \quad \frac{d\alpha}{dw} \approx \frac{1}{u_0}, \quad \Delta\alpha \sim \Delta\theta$$

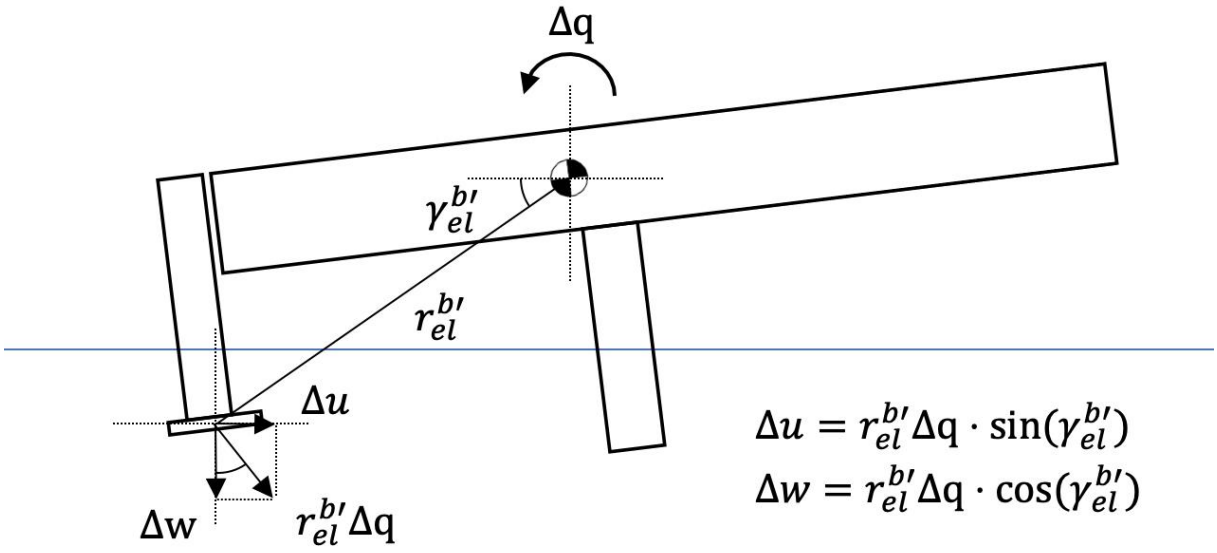

Figure 4.3: Effect of the angular velocity, q.

The terms denoted with (**) in Eq. 4.4 are the derivatives of the forces and moment to the pitch velocity, $\frac{\partial X}{\partial q}$, $\frac{\partial Z}{\partial q}$ and $\frac{\partial M}{\partial q}$. A change in pitch velocity around the CoG is experienced as a change in linear velocity $\Delta\overline{v}$ on every component. This velocity component $\overline{v}$ can be decomposed in a horizontal and vertical component, Δu and Δw, as is demonstrated in Fig. 4.3 for the elevator. Due to hydrodynamic lag this velocity $\overline{v}$ will however not be constant, but it will vary gradually over time as the flow needs time to settle to this new situation. This effect will be neglected and the change in velocity $\Delta\overline{v}$ as a result of a change in pitch, will be considered as a constant. Expressions for the derivatives to the two linear velocity components already exist, so that they can be used for an approximation for the pitch derivative. The linear velocities of every component separately, depend on the distance $r^{b'}$ to the CoG and on the angle of orientation $\gamma^{b'}$ around the y-axis. This means that every derivative has to be calculated separately, for every component. Using the approximation from Eq. 4.5 an approximation of $\frac{\partial M}{\partial q}$ is developed. This then takes the form of Eq. 4.6. The approach for $\frac{\partial Z}{\partial q}$ is similar. The individual derivatives are

afterwards summed to obtain the total derivative.

$$\begin{aligned}\frac{\partial M_i}{\partial q} &= \frac{\partial M_i}{\partial u}\frac{\partial u}{\partial q} + \frac{\partial M_i}{\partial w}\frac{\partial w}{\partial q} \\ &= \frac{\partial M_i}{\partial u} r_i^{b'} \sin(\gamma_i^{b'}) + \frac{\partial M_i}{\partial w} r_i^{b'} \cos(\gamma_i^{b'}) \\ &\approx \frac{\partial M_i}{\partial u} r_i^{b'} \sin(\gamma_i^{b'}) + \frac{1}{u_0}\frac{\partial M_i}{\partial \theta} r_i^{b'} \cos(\gamma_i^{b'})\end{aligned} \tag{4.6}$$

With $i =$ el,ru,zb.

$$\frac{\partial M}{\partial q} = \sum_i \frac{\partial M_i}{\partial q} \tag{4.7}$$

4.4 Stability Matrix

These approximations for the derivatives allow to construct the stability matrix A with only a limited amount of steady-state simulations. This will benefit simulation time a lot while still maintaining adequate accuracy. The stability matrix then becomes:

$$[A] = \begin{bmatrix} \frac{1}{m}\frac{\partial X}{\partial u} & \frac{1}{m}\frac{\partial X}{\partial z} & \frac{1}{m}\frac{\partial X}{\partial \theta} & \frac{1}{m}\frac{\partial X}{\partial w} & \frac{1}{m}\frac{\partial X}{\partial q} \\ 0 & 0 & 0 & 1 & 0 \\ 0 & 0 & 0 & 0 & 1 \\ \frac{1}{m}\frac{\partial Z}{\partial u} & \frac{1}{m}\frac{\partial Z}{\partial z} & \frac{1}{m}\frac{\partial Z}{\partial \theta} & \frac{1}{m}\frac{\partial Z}{\partial w} & \frac{1}{m}\frac{\partial Z}{\partial q} \\ \frac{1}{I_{yy}}\frac{\partial M}{\partial u} & \frac{1}{I_{yy}}\frac{\partial M}{\partial z} & \frac{1}{I_{yy}}\frac{\partial M}{\partial \theta} & \frac{1}{I_{yy}}\frac{\partial M}{\partial w} & \frac{1}{I_{yy}}\frac{\partial M}{\partial q} \end{bmatrix} \tag{4.8}$$

5 Methodology

This chapter gives more insight in the actual stability analysis of the Viper and the practicalities encountered. To obtain the necessary data for this analysis, the flow around the foils is simulated using CFD. The CFD simulations were calculated using the solver *Fluent* from *ANSYS* [14]. In order to get accurate results, good quality block-structured meshes are needed. These meshes were constructed using the *ANSYSICEM* software package.

5.1 Geometry

The geometry of the Viper was defined by the design of Goodall. As the flow will only be simulated below the water surface, just the elevator, Z-board and rudder will be simulated without the hull or sail. Relative positioning of the different foils is consequently important to get realistic results. This relative positioning was not always easy: neither foil is fixed on the hull as the rake of both foils can be adjusted according to sailing conditions. The relative positioning was done using the drawing in Fig. 5.1. Some overall dimensions are provided in Table 5.1. As the CoG can vary from setup to setup, the origin of the boat fixed frame is not constant. That is why a geometry-fixed reference frame is constructed. The origin of the geometry-fixed frame lies at the centre of the LE of the elevator when the rudder is in its neutral position, this is also shown in Fig. 5.1. The rudder is in its neutral position when the LE of its top section is parallel to the aft of the boat. This geometry-fixed frame will also be used to define the state of the boat.

The mass of the boat is known, but the position of the CoG is not. The position of the CoG

Table 5.1: The overall dimension of the foiling Viper.

Length	5 m
Beam	2.5 m
Mast height	8.5 m
Mainsail area	15 m^2
Jib area	3.7 m^2
Gennaker area	17.5 m^2
Mass	140 kg

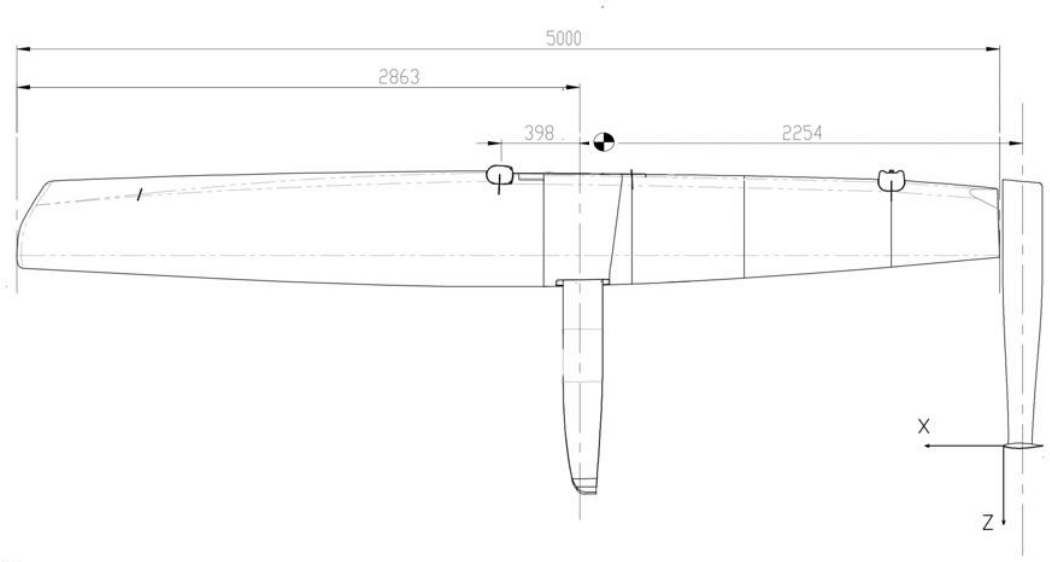

Figure 5.1: The Geometry of the boat.

is an important parameter in the stability analysis. The CoG is estimated by weighing all the heavy components of the boat (hull, beams, rudder+elevator, Z-board, mast) separately. As their relative position is known, the CoG was then easy to calculate using Eq. 5.1. This approximation (only considering the heavy components to calculate the CoG) was validated by checking where the CoG lied for a real boat. The results from the two approaches agreed remarkably well, with $x = 2.06$ m and $z = -1.54$ m as the coordinates for this CoG. The CoG is also displayed in Fig. 5.1. It lies above the platform as the mast (which is not displayed in the figure) is relatively long.

$$x_{cg} = \frac{\sum_i x_i * m_i}{\sum_i m_i} \tag{5.1}$$

Another parameter necessary for the stability analysis is the moment of inertia around the y-axis.

This was estimated by approximating all parts by rectangles with a uniform weight distribution. Again, only the heavy components are assumed (just as with the estimation of the CoG, as it lead to good results there). The moment of inertia was then calculated using the parallel-axis theorem as we know the weight and relative positioning of the different parts. This resulted in $I_{yy} = 3.20 \cdot 10^2\ kgm^2$.

$$I_{yy,CoG} = \sum_i (I_{cg,i} + m_i r_i^2) \tag{5.2}$$

With $I_{cg,i}$ = the moment of inertia of the rectangle around its CoG.; m_i = its mass and r_i = its relative position with respect to the CoG of the boat.

The calculation above does not take the crew into account. Each crew member has a weight of 70 kg and will be assumed to be a point mass. The CoG then shifts to $x = 1.98\ m$ and $y = -0.594\ mm$. The moment of inertia changes only slightly to $I_{yy} = 3.23 \cdot 10^2\ kgm^2$ as the crew members are positioned near the CoG.

5.2 Mesh

As the model assumes a symmetric boat only experiencing longitudinal motions, the flow at both sides of the boat will be symmetric. For this reason the mesh should only contain half the geometry. This results in 1 rudder, 1 elevator and 1 Z-board as our geometry. Simulating only half of the geometry will have a beneficial effect on calculation time. The CAD-files were provided by Goodall Design. Using these CAD-files the three parts (rudder, elevator and Z-board) are meshed separately using the *ICEM* software package from *ANSYS*. A fourth mesh contains a much larger surrounding background in which the three other meshes are combined using the overset functionality from *FLUENT*. *ICEM* is a very powerful tool to create block-structured meshes. This required lots of manual work so the meshing consequently took up a lot of time. In hindsight more use should have been made of the *replay scripts* to be able to make small adjustments to the mesh.

5.2.1 Overset

As was mentioned earlier the overset functionality of FLUENT will be used. Oversetting allows us to create three much 'simpler', separate meshes for the components together with a rectangular hexahedral background mesh in which they overlap. It has the advantage that the components meshes can be created independently. The solver will then, after initialization, remove overlap between the different meshes by deactivating redundant cells, these are then called *dead cells*. This happens based on cell size: the smallest cells will have the highest grid priority to maximize resolution. Apart from *dead cells* there are *solver*, *receptor* and *orphan cells*. A solution will tried to be obtained for the smallest local cell (i.e. solve cell). The larger mesh,

which then will not be solved at that location, will however still need values for those local cells. That are the so called *receptor cells* which are not solved themselves but get their values from the closest solve cell.
The background mesh can be much coarser than the part meshes, as in most locations the flow will remain undisturbed. Only in proximity to the foils and their meshes more refinement is needed. Special care should be taken to make sure that component meshes and background mesh have similar sizings in regions of overlap as this will give rise to better results for the overset initialization and consequent solutions. This is done by having a "bias" of the cell sizings towards the position of the component meshes. An example of this refinement can be seen in Fig. 5.2.

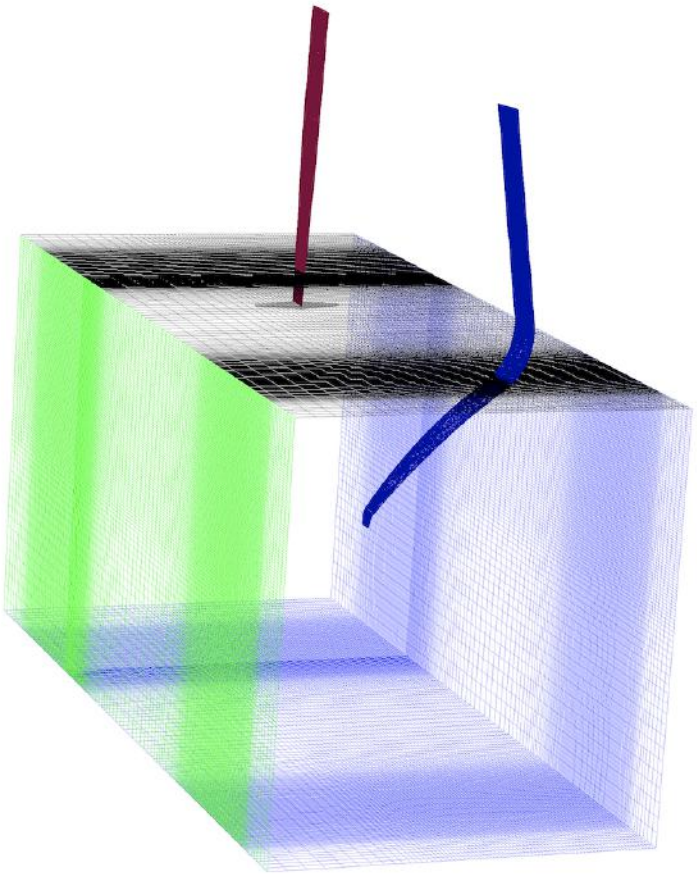

Figure 5.2: The components in the background mesh, with refinement towards the position of the components.

During initialization issues were encountered with orphan cells. Orphan cells are to be expected in regions were two walls are in proximity of one another and insufficient cells (less than 4)[15] are present in between the walls. In the case at hand there were three such regions: the region where the Z-board intersects the "rigid lid", the region where the rudder intersects the lid and

the region where the rudder and elevator are joined. Due to limited time no extra attention was spent to resolve this issue as it was noted that the effects on the forces were minor. The mentioned rigid-lid is the equivalent of the water surface, more on that later.
The different components can be rotated and translated independently, their relative positions define the *geometry*. The *standard geometry* has a rudder rake of -1 and a foil rake of 4. A rake is the relative angle of a component to the boat. Once this *geometry* is defined the three foils can also be translated and rotated as a whole, this to define a different *state*.

5.2.2 Components and background

The three components all have airfoil-like cross sections. The exact shapes and dimensions are not mentioned here to protect the work of Goodall Design. The three component meshes are all hexahedral C-grid meshes which extend sufficiently far downstream to resolve the wakes. Usual best practice is to make these C-grids sufficiently large (multiple chord lengths) to get accurate results. However, in this case the C-grids are not standalone grids, but rather component meshes in a background mesh for overset, so these meshes can be smaller. The C-grids have a radius of only 0.5 to 1 chord length. The first cell of the boundary layer of all three foils is located at 0.1 mm to have a y^+ value approximately between 30 and 300 on most of their surface. The y^+ value for more then 95% of the complete boundary layer lies in this range. There is however still room for improvement. The turbulence model will in this case make use of wall-functions to model the boundary layer. Originally y^+ values smaller than 5 were envisaged, to be able to calculate the BL without wall-functions. However, issues with inverted volume orientations were encountered over the whole surface of all foils. This issue likely had something to do with the *.IGS* files, used for importing the geometry. The outside boundary of all three C-grids will be of the overset-interface type. The components themselves are of course no-slip walls.

Rudder

The rudder has a length of 1350 mm and a chord length of 200 mm with symmetrical cross sections and a tapered bottom section. This is displayed in Fig. 5.3. As overset is used, it is opted to mesh the rudder and elevator separately as this leads to much simpler meshes. If they would not be meshed separately, the resulting T-structure would be very challenging to mesh using a block-structured grid. The rudder itself is the easiest component to mesh as this part can be meshed end to end without the tips needing to be meshed. The top end will always be above the water surface and the bottom end will form the connection with the elevator. A cross section of the mesh is given in Fig. 5.5. The complete rudder mesh contains $1.63 \cdot 10^6$ cells.

The elevator has a span of 420 mm and max chord length of 125 mm. The mesh now also has to be extended past the ends to simulate the vortices at the tips of the elevator. The mesh around this tip proved to be a rather complex task. In the original geometry the LE curved backwards at the tip, becoming tangent to the end surface. The tip was simplified to make meshing easier. This simplification is displayed in Fig. 5.4. For the final mesh the end surface of the elevator was meshed unstructured. This unstructured face mesh was then extruded to the overset interface.

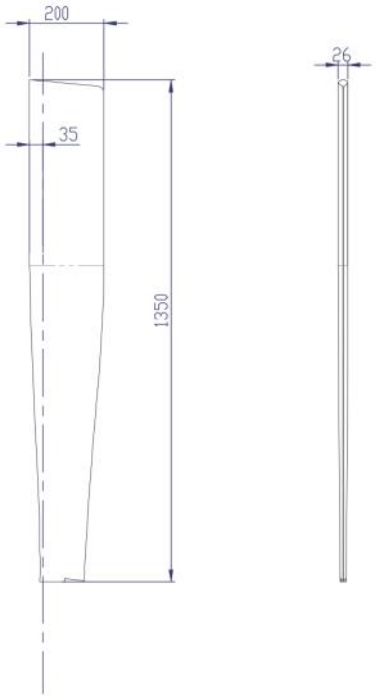

Figure 5.3: The rudder geometry.

This can be seen in Fig. 5.6 as the green grid extending from the elevator. The unstructured mesh was needed as the elevator ended in a sharp TE . A detail of the unstructured mesh can be seen in Fig. 5.7. The complete elevator mesh has $1.94 \cdot 10^6$ cells.

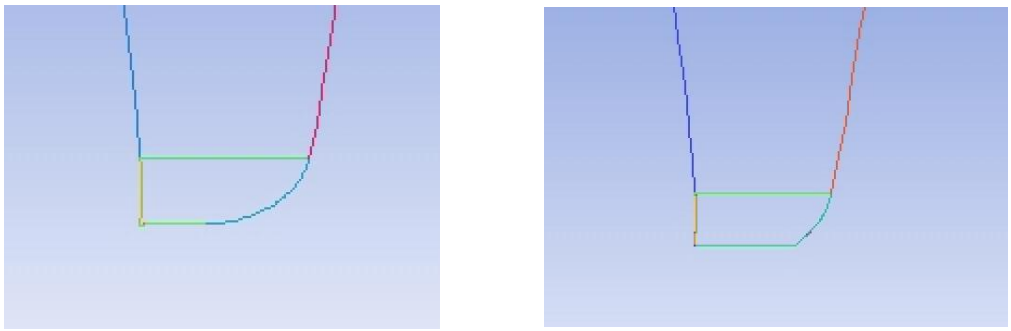

Figure 5.4: Left: Before simplification; Right: after simplification.

Elevator

Z-board

The Z-board's geometry is displayed in Fig. 5.8. The mesh should not be extended past the top end of the Z-board as this will always lie above the water surface in realistic operating conditions. At the bottom end the mesh is again extended past the tip with an unstructured mesh, similar to the elevator. The complete Z-board mesh has $1.44 \cdot 10^6$ cells.

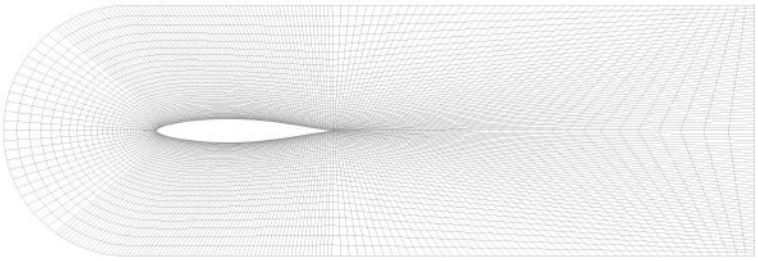

Figure 5.5: A cross section of the mesh of the rudder.

Background
It was chosen to model the free surface as a rigid "lid" rather than using a multi-phase flow method. This was chosen, as the influence of wave-making resistance is limited in this case, because there is no bulky hull piercing the water surface but rather two small, streamlined foils. This multi-phase approach would lead to much higher calculation times without a big increase in accuracy. Fig. 5.2 shows the background mesh together with the component meshes. The black surface represents the free surface modelled as a free-slip wall. The blue surfaces are pressure outlets which are tilted slightly inwards towards the outlet to prevent reversed flow on these surfaces. The green surface, which lies at the centre line of the boat, is modelled as a symmetry plane. This background mesh is completed with a velocity inlet and pressure outlet at the ends which are omitted in the figure. The complete background has $2.18 \cdot 10^6$ cells.

5.3 Solver

Fluent is a very powerful and versatile tool for simulating flow-problems. To control the software, there are two possibilities: using the GUI (graphical user-interface) or otherwise using the TUI (text user-interface) . The GUI is a good way to experiment with the program and was used to get to know all its necessary functionalities. Later on, to be able to run various simulations consecutively, *journal files* were loaded into the TUI. These *journal files* contained FLUENT commands and could be coded using the coding language *Scheme*. These *journal files* also allowed to code more complex simulations, e.g. simulations requiring loops. A further functionality of FLUENT are the *User-Defined Functions* or *UDFs*. These UDFs are a very

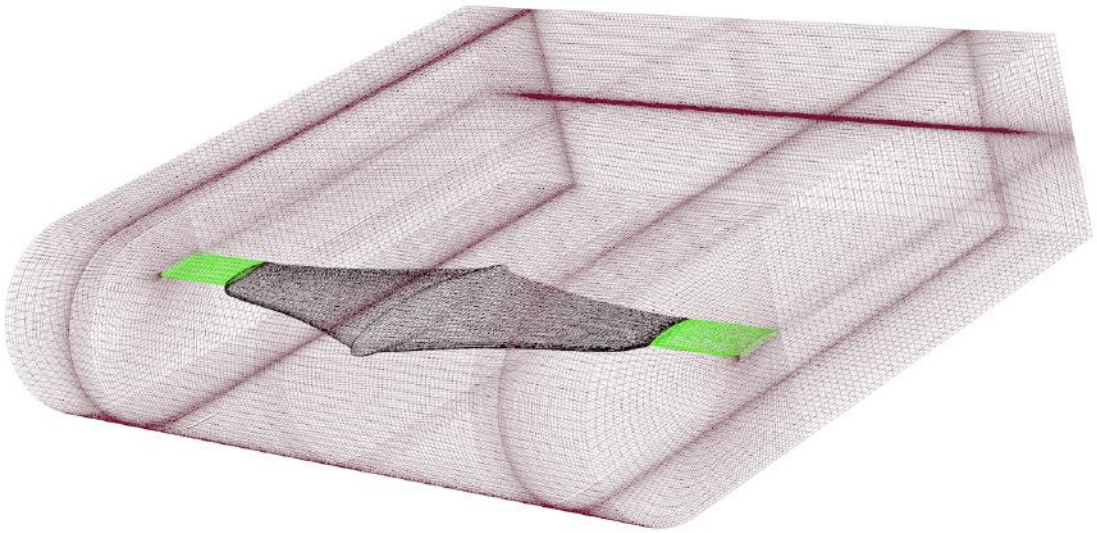

Figure 5.6: The complete elevator mesh with the unstructured block highlighted.

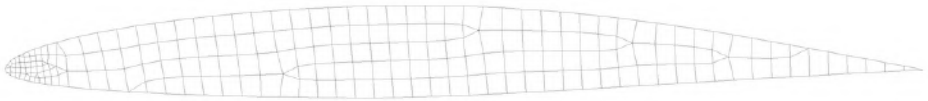

Figure 5.7: A detail of the unstructured block.

powerful tool within FLUENT to extend FLUENT's standard capabilities. E.g. it allows to translate and rotate the mesh, define pressure profiles on outlets, extract forces and moments from parts, ... These UDFs are coded using *C*.
The speed range in which foiling is to be expected lies above 5 m/s and the foils have chord lengths of 0.2 m, meaning Reynolds numbers will always lie well above 10^6, even for low-speed conditions. Turbulence will be modeled using the $k-\omega$ SST model. At the velocity inlet the turbulent intensity is set to 1% and the viscosity ratio $\frac{\mu_t}{\mu}$ is set to 1, these are typical values for external flow problems [16]. To include the effects of hydrostatic pressure gravity g is enabled and a hydrostatic pressure profile is imposed at the pressure outlets.

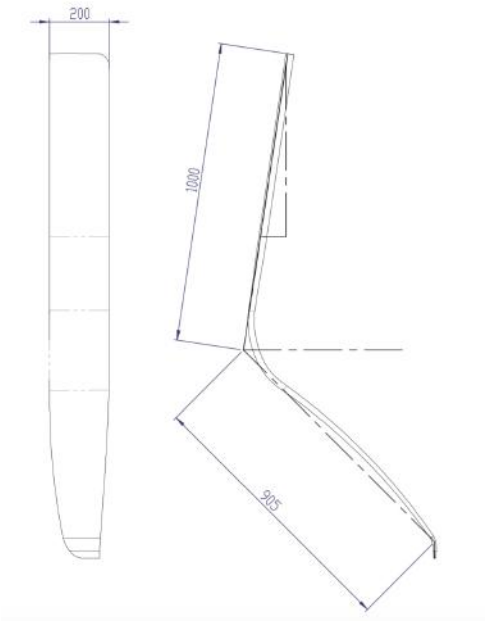

Figure 5.8: The overall dimensions of the Z-board.

5.4 Equilibrium state

As the stability matrices defined in chapter 4 are only valid around an equilibrium state, a very important step in analyzing stability is calculating this equilibrium state. To this end an algorithm was developed and implement using both journal files and UDFs.

5.4.1 External forces and moments

As only forces and moments resulting from the foils below the water surface will be calculated, external forces and moments which are not calculated should be estimated in order to find a realistic equilibrium point. For the force balance the weight of boat (140 kg) together with the weight of the crew (140 kg) should be included, adding up to 280 kg. As only half of the boat is modelled only half of this weight should be included. For the moment balance the moment generated by the sail M_{sail} around the centre of gravity has to estimated. Note that the moment generated by the weight of the crew should not be included as the weight of the crew was already included in the calculation for the position of the CoG and the moment of inertia. The moment generated by the sail can be estimated fairly accurate. The drag generated by the foils follows from the CFD calculations, e.g. the drag generated for half a boat at 10 m/s is equal to $2.15 \cdot 10^2$ N. The sail should deliver a force which is equal in magnitude but opposite in direction to this drag. From data from Goodall Design it is known that the point of application of the sail lies approximately 3.25 m above the centre of gravity. These values are then used to get an estimation of the moment M_{sail} of the sail.

5.4.2 Algorithm

The *geometry* can vary by changing the rudder rake, foil rake, position of the CoG... The relative draft Δz and relative trim angle $\Delta\theta$ of the boat as a whole defines a *state*. The goal of the algorithm is to find a state (Δz, $\Delta\theta$) for which the total force and the total moment of the geometry are zero. This relative draft and trim are defined in reference to a arbitrary chosen initial state. The algorithm discussed here is based on the *Newton-Rhapson* method for 2 variables. This root-finding method is expressed generally in eq. 5.3. In every step the force and moment is calculated using CFD. These values are then used to estimate where the force and moments will be zero ($F = M = 0$) using Newton-Rhapson. The boat is then moved to this new state and this is continued until the force and moment are zero (or below a certain convergence threshold).

$$\begin{bmatrix} z \\ \theta \end{bmatrix}_{n+1} = \begin{bmatrix} z \\ \theta \end{bmatrix}_{n} - [J]^{-1} \begin{bmatrix} F \\ M \end{bmatrix}_{n} \tag{5.3}$$

The estimation of the state where the force and moment will become zero is based on the derivatives of the force and moment to the draft and trim. In every step derivatives of both the force and the moment to both the draft and the trim angle are calculated, i.e. $\frac{\delta F}{\delta \theta}$, $\frac{\delta F}{\delta z}$, $\frac{\delta M}{\delta \theta}$ and $\frac{\delta M}{\delta z}$. For every state the flow is simulated and the forces and moments of the three foils are calculated. Together with the external forces and momenta, they form the total force F and total moment M on the boat. From this total force and moment the derivatives can be calculated in between different iterations using finite differencing. These derivatives are placed in a matrix J called the *Jacobian*.

However if both draft and trim angle are updated simultaneously there is no way of calculating the derivatives, as the individual contributions of both the draft and trim cannot be distinguished. That is why a segregated approach is proposed. Every iteration consists of two sub-iterations: one iteration for the draft update Δz and one for the trim angle update $\Delta\theta$. This gets demonstrated in Eq. 5.4.

$$
\begin{aligned}
&\underline{i = k} \quad \begin{bmatrix}\Delta z \\ \Delta\theta\end{bmatrix} = \begin{bmatrix}(\frac{\delta Z}{\delta z})_{k-1} & (\frac{\delta Z}{\delta \theta})_k \\ (\frac{\delta M}{\delta z})_{k-1} & (\frac{\delta M}{\delta \theta})_k\end{bmatrix}^{-1} \begin{bmatrix}(-Z)_k \\ (-M)_k\end{bmatrix} \\
&\quad \bullet\ \underline{i = k+1} \qquad \text{perform} \quad \Delta z \\
&\qquad\quad \rightarrow \text{calculate } (Z)_{k+1}, (M)_{k+1} \\
&\qquad\quad \rightarrow \text{calculate } (\frac{\delta Z}{\delta z})_{k+1}, (\frac{\delta M}{\delta z})_{k+1} \\
&\quad \bullet\ \underline{i = k+2} \qquad \text{perform} \quad \Delta\theta \\
&\qquad\quad \rightarrow \text{calculate } (Z)_{k+2}, (M)_{k+2} \\
&\qquad\quad \rightarrow \text{calculate } (\frac{\delta Z}{\delta \theta})_{k+2}, (\frac{\delta M}{\delta \theta})_{k+2} \\
&\underline{i = k+2} \quad \begin{bmatrix}\Delta z \\ \Delta\theta\end{bmatrix} = \begin{bmatrix}(\frac{\delta Z}{\delta z})_{k+1} & (\frac{\delta Z}{\delta \theta})_{k+2} \\ (\frac{\delta M}{\delta z})_{k+1} & (\frac{\delta M}{\delta \theta})_{k+2}\end{bmatrix}^{-1} \begin{bmatrix}(-Z)_{k+2} \\ (-M)_{k+2}\end{bmatrix} \\
&\quad \bullet\ \underline{i = k+3} \qquad \text{perform} \quad \Delta z \\
&\qquad\quad \rightarrow \text{calculate } (Z)_{k+3}, (M)_{k+3} \\
&\qquad\quad \rightarrow \text{calculate } (\frac{\delta Z}{\delta z})_{k+3}, (\frac{\delta M}{\delta z})_{k+3} \\
&\quad \bullet\ \underline{i = k+4} \qquad \text{perform} \quad \Delta\theta \\
&\qquad\quad \rightarrow \text{calculate } (Z)_{k+4}, (M)_{k+4} \\
&\qquad\quad \rightarrow \text{calculate } (\frac{\delta Z}{\delta z})_{k+4}, (\frac{\delta M}{\delta z})_{k+4}
\end{aligned}
\tag{5.4}
$$

In iteration k the draft Δz and trim $\Delta\theta$ updates are calculated. To be able to distinguish their individual contributions to the force and moment they get executed separately in iteration $k+1$ and $k+2$. in iteration $k+1$, the draft gets updated using the draft update Δz calculated in iteration k. The flow for this new state gets solved and from the resulting new force and moment, $(Z)_{k+1}$ and $(M)_{k+1}$, the derivatives to the draft are updated using finite differencing. This same procedure is repeated for the trim angle $\Delta\theta$ in iteration $k+2$. After the state of iteration $k+2$ is simulated, the *Jacobian* together with the force and moment are updated based on the derivatives calculated in iteration $k+1$ and $k+2$. This method allows to calculate the derivatives and update the state simultaneously. To initialize this algorithm, the jacobian needs to be constructed. To this end the force and moment of the initial state is calculated together with the force and moment of two additional states. These two additional state are each characterized by either an update for the draft or trim.

5.4.3 Implementation

The algorithm above is implemented in FLUENT using *journal files* and *UDFs*. To be able to make easy adjustments different journal files are created to do various tasks.

One journal file is responsible for developing the geometry. In this journal the component meshes and background mesh are loaded into FLUENT and their relative positioning is set up. This mesh now defines a geometry in an arbitrary state. All this then gets saved to a case-file. This way various geometries can be created and saved with relative ease. The geometry in this state will be used for the zeroth iteration in the algorithm.
A UDF file is created which contains various functions needed for the algorithm above. There are 5 kinds of functions used:

1. A function for extracting the forces and momenta for the 3 foils and, using the external forces, calculating the total forces and momenta.
2. Functions for calculating the derivatives from the total forces and momenta.
3. Functions for calculating the motions based on the Jacobian.
4. A function to perform the mesh movement.
5. A function to define the hydrostatic pressure profiles at the pressure outlets.

A main journal file lets Fluent load the case-file containing the defined geometry and the UDF-library. This main journal file is also responsible of defining the right settings in FLUENT, e.g. initialization settings, convergence thresholds, turbulence models, ... This file also creates the overset mesh and dynamic mesh. A dynamic mesh allows to move the various component meshes in the background mesh. A loop inside this main journal is the actual implementation of the algorithm. After the complete setup is prepared and the case is initialized, a first simulation is done to get the initial values of the total force Z and moment M. Then separately two initializing motions for the trim angle θ and draft z are carried out. The flow is then simulated again for these two new states and the resulting total force and moment are extracted using the UDFs. From this force and moment and the force and moment of the zeroth iteration a first Jacobian matrix can be created for that particular point. This Jacobian then results in the first motions which also will be carried out to calculate new derivatives. This process is then repeated until the total force and moment are below a certain threshold value.

The implementation of the algorithm was initially developed for a 2-dimensional case. This 2D case contained an asymmetric profile and smaller symmetric profile downstream (as is usual for a stable setup). For this case only an equilibrium for the moment had to be found as the lift of this 2D case did not depend on the draft. This 2D case was very helpful to get the principles of the algorithm right and proved the algorithm converged to valid equilibrium. Afterwards this code was extended to support a 3D case.

5.5 Issues

Soon it was noted how much longer the 3D case took to converge. To limit calculation time the convergence thresholds for turbulent kinetic energy k and dissipation rate ω in FLUENT were given rather high values (10^{-3}). This was deemed necessary to be able to validate the algorithm in a limited amount of time. However after a while it became clear that the algorithm in 3D did not converge to a result.

5.5.1 Validation

To make sure the handled *standard geometry* from sec. 5.2.1 is in fact a stable geometry, values for the the total moment and total force were calculated over finite range of relative drafts z and trim angles θ without making use of a dynamic mesh and defining every state directly using a journal file. These simulations were run with lower convergence thresholds (10^{-5}). Starting from an starting state, the geometry was simulated for 5 different relative drafts z and for 5 different relative trim angles θ. This results in 25 points. The starting state is defined making use of the geometry-fixed axes from sec. 5.1. The starting state has a zero trim angle and a 100 mm draft. This means that the rudder is submerged for 100 mm as the origin lies at the bottom of the rudder. The results are plotted in Fig. 5.9. In this figure 2 surfaces are displayed: the red surface for the total moment and the blue surface for the total force. These surfaces are completed with iso-curves to get an idea of the level. The iso-curves at 0 N or 0 Nm are displayed in black.

The first thing which becomes clear from this figure is that there is in fact an equilibrium point as the two black iso-curves intersect. In this point, ($z = 0.1589, \theta = -2.381°$), both force and moment are zero (or at least somewhere near this point) and an equilibrium state exists. Further it can be noted how the moment is mainly dependant on the trim angle and only in a lesser extent to the draft and how the force is dependant on both the trim angle and the draft. This becomes more clear in Fig. 5.10 and Fig. 5.11.

Static stability of an equilibrium state means that when the boat experiences a deviation away from this equilibrium, the force and moment will vary in such a way that the boat is forced back to this equilibrium. It can be seen from Fig. 5.10 that if the draft increases (boat moves deeper into the water), the force becomes negative meaning that more lift is generated and the hull moves back up again. Remember that the Z-axis is directed downwards. From Fig. 5.11 it can be seen that if the trim angle increases (nose up), a nose-down (negative) moment is generated. The equilibrium state is consequently statically stable.

Convergence criteria

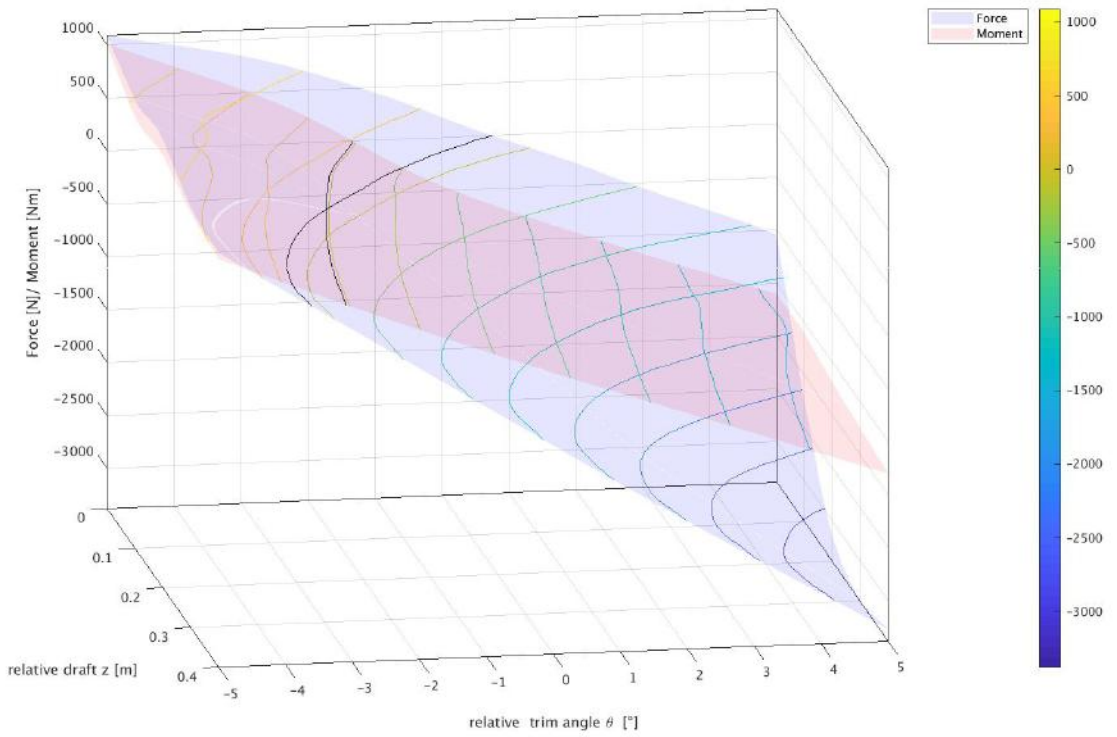

Figure 5.9: A surface plot of the of the force and moment of the Viper as a function of the relative draft z and the relative trim angle θ.

The fact that an equilibrium state exists, but that the algorithm does not converge to this state means that the reason for not converging has to be found elsewhere. By simulating the flow for points around this equilibrium state, some anomalies were discovered. There was noticed how simulating two identical states can lead to two very different values for both the force and the moment. The reason for this discrepancy lies in the fact that the solution of the previous simulation influences the solution of the current simulation. For steady-state simulation this cannot be the case. This implies that the higher convergence thresholds are partly responsible for preventing the algorithm from converging. This is demonstrated in Table 5.2. Two simulations of an identical state were performed but with a different convergence threshold. Both these simulations were initialized in the same way to have no influence of a previous simulation. A slight difference of the threshold value leads to an 8% change for both the force and the moment relative to the ranges for the force and moment from Fig. 5.9. This means that the simulations are nowhere near being converged.

This prevents the algorithm from working: a small change in either the draft or the trim angle, can lead to very unpredictable behaviour for the force and moment. E.g. the values in Table 5.2 would lead to infinite values for the derivatives. This leads to a very inconsistent Jacobian matrix. Normally this Jacobian is expected to have nearly constant values near an equilibrium

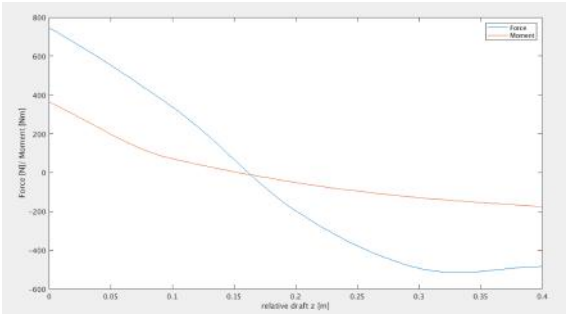

Figure 5.10: Force and moment as a function of the draft Δz for the equilibrium trim θ_0.

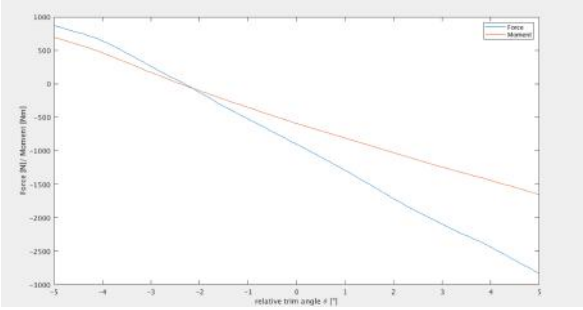

Figure 5.11: Force and moment as a function of the trim angle $\Delta\theta$ for the equilibrium draft z_0.

Table 5.2: Forces and moments calculated using two different convergence thresholds.

Convergence thres. for k [J/kg]	**Force [N]**	**Moment [Nm]**
0.001	159	-115
0.002	479	100

point as the force and moment surfaces are expected to be smooth. This means that the algorithm will initially show good behaviour for as long as the derivatives are calculated using sufficiently large steps for the draft and trim. However, the more the algorithm approaches the equilibrium state, the smaller the steps will be. This will lead to more inconsistent behaviour for the Jacobian and will cause the algorithm to diverge. Unfortunately there was not enough time to run the algorithm with lower convergence thresholds.

As the surfaces in Fig. 5.9 are calculated with lower convergence thresholds, and by using sufficiently large steps, the resulting surfaces are a good representation of the reality. This means that they can be used to approximate an equilibrium state for the standard geometry.

5.6 Derivatives

Once the equilibrium state for a geometry and setup is found, the stability matrix needs to be constructed. The calculations for the derivatives, necessary for constructing the stability matrix, are rather straightforward. As was demonstrated in the previous chapter only 3 kinds of derivatives need to be calculated to construct the longitudinal stability matrix. The force X, the force Z and the moment M each have to be derived to the trim θ, to the forward velocity/surge u and the draft z. They are calculated using finite differencing around the equilibrium state. Together with the forces and moment from the equilibrium state (which are supposed to be approximately zero), three additional sets of the forces and moment are calculated. This is done by three additional states: one for the draft, one for the trim and on for the surge. This is

Table 5.3: The relative position and orientation of the components in the stability axes.

.	rudder (i=ru)	elevator (i=el)	Z-board (i=zb)	units
$r_i^{b'}$	2.46E+00	2.55E+00	1.49E+00	$[m]$
$\gamma_i^{b'}$	34.7	37.0	103.0	$[^\circ]$

demonstrated in Eq. 5.5:

$$\frac{\delta A}{\delta \theta} = \frac{A_1 - A_0}{\theta_1 - \theta_0}; \quad \frac{\delta A}{\delta z} = \frac{A_2 - A_0}{z_2 - z_0}; \quad \frac{\delta A}{\delta u} = \frac{A_3 - A_0}{u_3 - u_0}. \tag{5.5}$$

with: $A = X, Z$ or M
$0 \rightarrow$ equilibrium state
$1 \rightarrow$ state with trim update $\Delta\theta$
$2 \rightarrow$ state with draft update Δz
$3 \rightarrow$ state with surge update Δu

To calculate the derivatives to heave and pitch, the approximations from previous the chapter are used. The approximation for the pitch has to be calculated for every component separately as this derivative depends on the individual positioning of the component. This means that the forces and moment have to be calculated individually for every component.The position and orientation of the different components of the standard geometry, in the equilibrium state, are shown in Table 5.3. These values are necessary for the approximations.

The equations used for the approximation are repeated here:

$$\frac{\delta A}{\delta w} = \frac{\delta A}{\delta \theta}\frac{\delta \theta}{\delta w} = \frac{\delta A}{\delta \theta}\frac{\delta \alpha}{\delta w} \approx \frac{1}{u_0}\frac{\delta A}{\delta \theta} \qquad \text{With } A = X, Z, M \tag{5.6}$$

$$\begin{aligned} \frac{\delta A_i}{\delta q} &= \frac{\delta A_i}{\delta u}\frac{\delta u}{\delta q} + \frac{\delta A_i}{\delta w}\frac{\delta w}{\delta q} \\ &= \frac{\delta A_i}{\delta u} r_i^{b'} sin(\gamma_i^{b'}) + \frac{\delta A_i}{\delta w} r_i^{b'} cos(\gamma_i^{b'}) \\ &\approx \frac{\delta A_i}{\delta u} r_i^{b'} sin(\gamma_i^{b'}) + \frac{1}{u_0}\frac{\delta A_i}{\delta \theta} r_i^{b'} cos(\gamma_i^{b'}) \end{aligned} \tag{5.7}$$

With $i =$ el,ru,zb.

$A = X, Z, M$

$$\frac{\delta A}{\delta q} = \sum_i \frac{\delta A_i}{\delta q} \tag{5.8}$$

This then results in 6 additional derivatives. The derivative of the force X to the pitch is so small, it becomes negligible.

6 Results

As time was limited, only one equilibrium state was calculated. This means that only one set of stability derivatives is available to discuss. These derivatives will be used to construct a stability matrix and to determine the eigenmodes. The way these derivatives are calculated is already discussed in the previous chapters. The eigenmodes can be used the asses the stability performance of the Viper in this particular state. The equilibrium state under consideration is that of the standard geometry sailing at a speed of 10 m/s. The standard geometry has a rudder rake of $-1°$ and Z-board rake of $4°$.

6.1 Equilibrium state

Using the geometry-fixed frame, the equilibrium state has a draft of $z = 0.259\ m$, and a trim of $\theta = -2.38°$. As was mentioned in the previous chapter this position is approximated from the surface plot of the force Z and moment M. This surface plot is repeated here in Fig. 6.1. The equilibrium state can be found where the two zero, black iso-curves intersect. In Fig. 6.2 the geometry can be found in its equilibrium state relative to the free surface.

6.2 Derivatives

As there was not enough time to run the equilibrium algorithm with lower convergence thresholds, the derivatives were calculated around the equilibrium state resulting from the surface plots. The derivatives are calculated with the forces and moments from the individual components re-

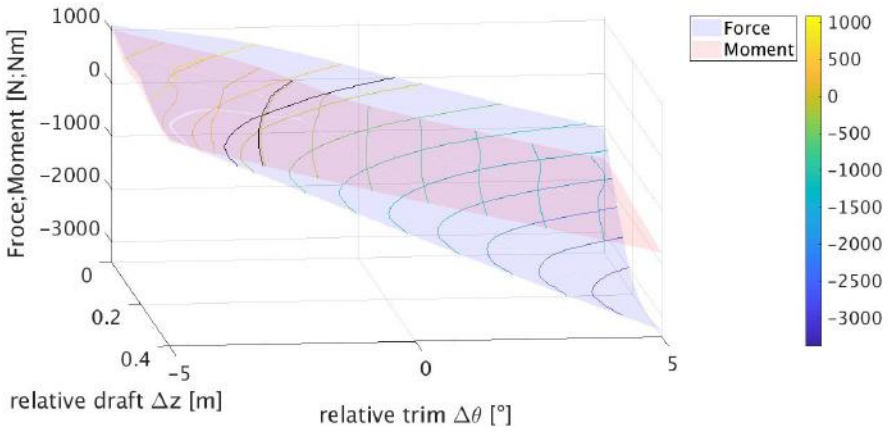

Figure 6.1: A surface plot of the of the force Z and moment M of the Viper as a function of the relative draft z and the relative trim angle θ, referenced to the starting state.

sulting from the simulations using finite differencing. The individual component derivatives are given in Table 6.1. The resulting general derivatives are tabulated in table 6.2 and 6.3.

Table 6.1: The derivatives of the individual components around the equilibrium state from the standard geometry at a speed of 10 m/s.

	elevator	rudder	Z-board	units
$\frac{\delta Z}{\delta \theta}$	-8.88E+01	1.04E+00	-2.94E+02	$[N/rad]$
$\frac{\delta Z}{\delta z}$	-3.56E+01	1.51E+01	-7.99E+03	$[N/m]$
$\frac{\delta Z}{\delta u}$	2.41E+01	4.05E-01	-3.38E+02	$[N \cdot s/m]$
$\frac{\delta M}{\delta \theta}$	-2.08E+02	3.87E-01	-1.44E+01	$[N/rad]$
$\frac{\delta M}{\delta z}$	-1.19E+02	-3.45E+01	-8.86E+02	$[N/m]$
$\frac{\delta M}{\delta u}$	5.15E+01	-7.91E-01	-4.88E+01	$[N \cdot s/m]$

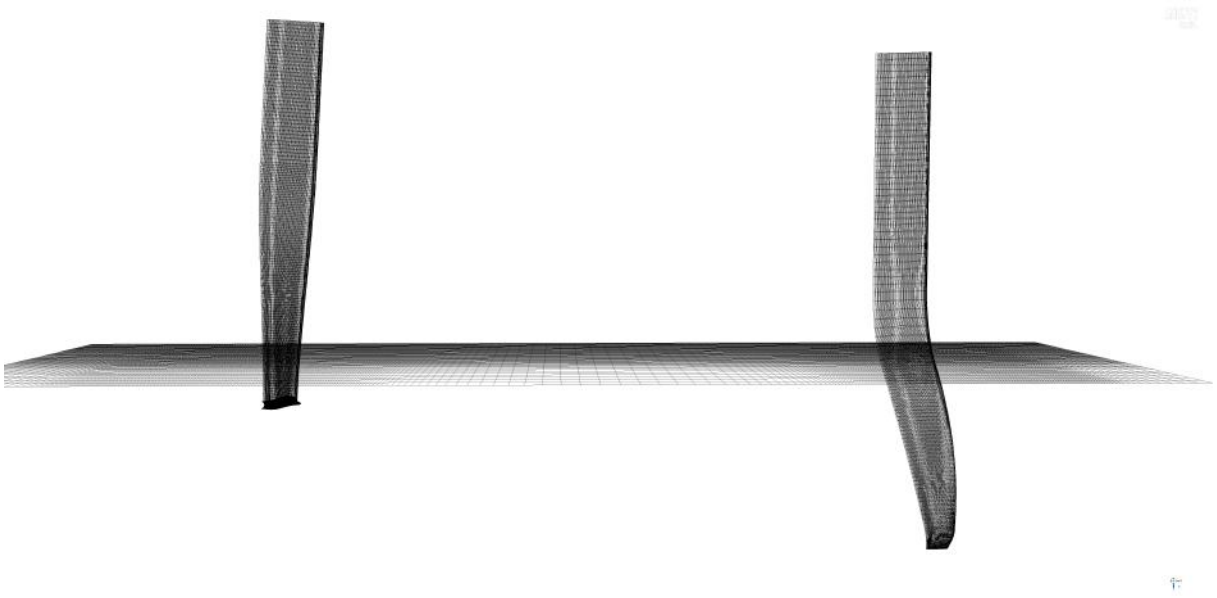

Figure 6.2: A visualisation of the equilibrium state relative to the free surface.

Table 6.2: The derivatives around the equilibrium state from the standard geometry at a speed of 10 m/s.

derivative	value	units
$\frac{\delta X}{\delta \theta}$	-6.98E+02	[N/rad]
$\frac{\delta X}{\delta z}$	-3.09E+02	[N/m]
$\frac{\delta X}{\delta u}$	3.76E+01	[N ·s / m]
$\frac{\delta Z}{\delta \theta}$	-2.19E+04	[N/rad]
$\frac{\delta Z}{\delta z}$	-8.01E+03	[N/m]
$\frac{\delta Z}{\delta u}$	-3.13E+02	[N ·s / m]
$\frac{\delta M}{\delta \theta}$	-1.27E+04	[N/rad]
$\frac{\delta M}{\delta z}$	-1.04E+03	[N/m]
$\frac{\delta M}{\delta u}$	1.92E+00	[N ·s / m]

Table 6.3: The derivatives for heave and pitch around the equilibrium state from the standard geometry at a speed of 10 m/s, calculated using the approximations from chapter 4.

derivative	value	units
$\frac{\delta X}{\delta w}$	-6.98E+01	$[N \cdot s/m]$
$\frac{\delta X}{\delta q}$	-	$[N \cdot s/rad]$
$\frac{\delta Z}{\delta w}$	-2.19E+03	$[N \cdot s/m]$
$\frac{\delta Z}{\delta q}$	-5.09E+02	$[N \cdot s/rad]$
$\frac{\delta M}{\delta w}$	-1.27E+03	$[Nm \cdot s/m]$
$\frac{\delta M}{\delta q}$	-2.70E+01	$[Nm \cdot s/rad]$

6.3 Longitudinal Stability

The goal of all previous chapters was to construct the longitudinal stability matrix. This matrix is used to asses the dynamic stability of the boat around a certain equilibrium state. This allows to compare different geometries and conditions. Based on these comparisons the stability can be improved. The longitudinal stability matrix is repeated below:

$$[A] = \begin{bmatrix} \frac{1}{m}\frac{\delta X}{\delta u} & \frac{1}{m}\frac{\delta X}{\delta z} & \frac{1}{m}\frac{\delta X}{\delta \theta} & \frac{1}{m}\frac{\delta X}{\delta w}^{*} & \frac{1}{m}\frac{\delta X}{\delta q}^{**} \\ 0 & 0 & 0 & 1 & 0 \\ 0 & 0 & 0 & 0 & 1 \\ \frac{1}{m}\frac{\delta Z}{\delta u} & \frac{1}{m}\frac{\delta Z}{\delta z} & \frac{1}{m}\frac{\delta Z}{\delta \theta} & \frac{1}{m}\frac{\delta Z}{\delta w}^{*} & \frac{1}{m}\frac{\delta Z}{\delta q}^{**} \\ \frac{1}{I_{yy}}\frac{\delta M}{\delta u} & \frac{1}{I_{yy}}\frac{\delta M}{\delta z} & \frac{1}{I_{yy}}\frac{\delta M}{\delta \theta} & \frac{1}{I_{yy}}\frac{\delta M}{\delta w}^{*} & \frac{1}{I_{yy}}\frac{\delta M}{\delta q}^{**} \end{bmatrix} \tag{6.1}$$

The stability matrix for the standard geometry evaluated for the equilibrium state results in the matrix below. This is done using the data from sec. 6.2.

$$[A] = \begin{bmatrix} -0.27 & -2.21 & -4.99 & -0.50 & 0.00 \\ 0 & 0 & 0 & 1.00 & 0 \\ 0 & 0 & 0 & 0 & 1.00 \\ -2.24 & -57.20 & -156.21 & -15.62 & -6.51 \\ 0.01 & -6.42 & -78.59 & -7.86 & -14.75 \end{bmatrix} \tag{6.2}$$

6.3.1 Eigenmodes

Using *MATLAB* the eigenvalues and eigenvectors are easily determined. The eigenvalues will determine the general behaviour of each mode, and the eigenvectors will determine the amplitude and phase of each variable. The matrix above results in one real eigenvalue, and two complex conjugated pairs. These eigenvalues are listed below and are visualised in the root locus diagram in Fig. 6.3. There is one real eigenvalue and two complex conjugated pairs of eigenvalues.

$$\lambda_{1,2} = -14.42 \pm 6.95i$$
$$\lambda_{3,4} = -0.812 \pm 3.60i$$
$$\lambda_{5} = -0.178$$

All the eigenvalues have a negative real part: this leads to the conclusion that the Viper is *dynamically stable* for the chosen geometry and speed. An eigenmode is defined by the multiplication of the eigenvector with the exponential of the respective eigenvalue:

$$\Delta x_i = v_i e^{\lambda_i t} \qquad \text{with } i = 1, ..., 5 \tag{6.3}$$

From this definition it can be seen that the mode will dampen out exponentially in time if the real part of the eigenvalue is negative. If the eigenvalue becomes more negative, the mode will

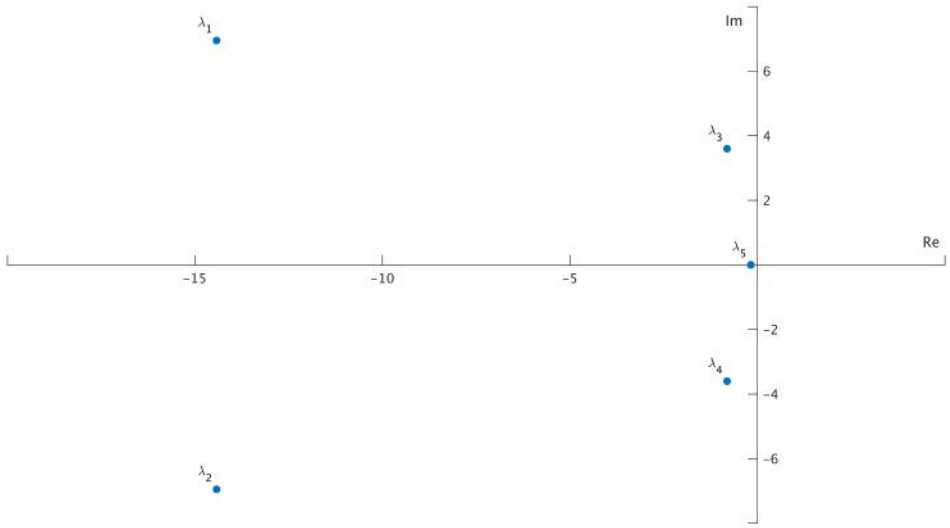

Figure 6.3: Root locus diagram for the Viper in the equilibrium of the standard geometry.

be dampened even more quickly. This can be expressed making use of the *half-life* $t_{\frac{1}{2}}$. This is the time elapsed until the original amplitude has decayed to half its original value.

$$t_{\frac{1}{2},i} = \frac{ln(0.5)}{Re(\lambda_i} \tag{6.4}$$

This is an interesting measure to compare the five eigenvalues. The half-lives are $t_{\frac{1}{2};1} = t_{\frac{1}{2};2} = 4.81 \cdot 10^{-2}\ s$; $t_{\frac{1}{2};3} = t_{\frac{1}{2};4} = 8.54 \cdot 10^{-1}\ s$ and $t_{\frac{1}{2},5} = 3.89\ s$. In the case that the eigenvalue is complex, the eigenmode will have an oscillating component as $e^{ix} = cos(x) + i \cdot sin(x)$. This oscillation is sinusoidal and will have a period determined by

$$T_i = \frac{2\pi}{Im(\lambda_i)} \tag{6.5}$$

For the complex eigenvalues this results respectively in $T_1 = T_2 = 0.904\ s$ and $T_3 = T_4 = 1.75\ s$. The eigenmode will simultaneously be influenced by the eigenvector. If the eigenvalue is complex the eigenvector will be so too. The eigenvectors are given below:

$$v_1 = \overline{v_2} \begin{Bmatrix} 0.0039 - 0.0199i \\ -0.0371 + 0.0154i \\ -0.0429 - 0.0207i \\ 0.4274 - 0.4805i \\ 0.7630 + 0.0000i \end{Bmatrix}; \quad v_3 = \overline{v_4} = \begin{Bmatrix} 0.0397 + 0.0074i \\ -0.0535 - 0.2372i \\ -0.0564 + 0.0771i \\ 0.8976 + 0.0000i \\ -0.2320 - 0.2658i \end{Bmatrix}; \quad v_5 = \begin{Bmatrix} 0.9986 \\ -0.0510 \\ 0.0035 \\ 0.0091 \\ -0.0006 \end{Bmatrix}$$

Taking a look at the real eigenvector v_5 in Fig. 6.4, some characteristics of the behaviour of the eigenmode Δx_5 can be recognized. An increase in speed Δu is associated with a decrease in draft

Δz (meaning that the boat gets lifted from the water). This corresponds to what behaviour was expected as an increase in speed will generate more lift on the foils. As the equilibrium trim θ_0 is $-2.381°$ and as the elevator has a negative rake, the additional lift generated by the elevator will be directed downwards resulting in positive moment. This is translated in a slight increase in trim angle $\Delta\theta$, meaning that the boat will be tilted more *nose-up*. The draft variation Δz occurs naturally together with a heave variation Δw. As this is a real mode, a draft and trim variation resulting from a speed variation will happen without any overshoot. From the half-lives it can be seen that it will take 3.89 s until the boat is halfway to its new equilibrium.

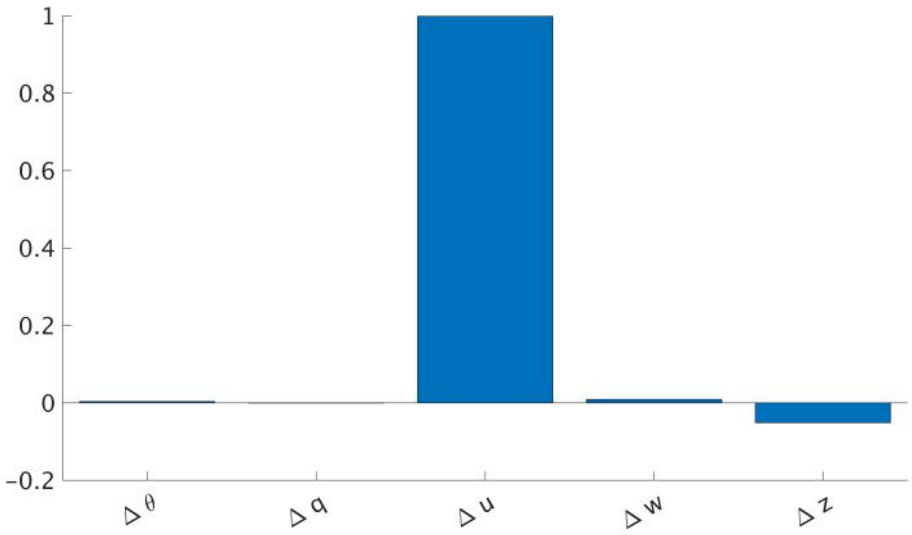

Figure 6.4: A visualisation of the real eigenvector v_5.

The combination of the eigenmodes Δx_1 and Δx_2 will be a heavily damped, sinusoidal motion dominated by a variation in heave Δw and pitch Δq. This will resemble some kind wobbling. After the boat moves downwards, it will start to tilt more nose up. This will result in more lift, meaning that the boat will eventually start moving up again. Hence the oscillatory motion. The heave and pitch motion are almost in phase with each other. This mode has a half-life of $t_{\frac{1}{2};1} = t_{\frac{1}{2};2} = 4.81 \cdot 10^{-2}$ s and a period of $T_1 = T_2 = 0.904$ s.

The combination of the eigenmodes Δx_3 and Δx_4 will be a weakly damped, sinusoidal motion again dominated by a variation in heave Δw and pitch Δq. The half-life is $t_{\frac{1}{2};3} = t_{\frac{1}{2};4} = 8.54 \cdot 10^{-1}$ s and the period $T_3 = T_4 = 1.75$ s. As the half-life and period are larger in this case, the variation in trim angle $\Delta\theta$ and draft Δz resulting from the variation in heave and pitch will be more outspoken. This is demonstrated by the larger vector components for trim and draft in Fig. 6.6. The heave and pitch variation are now nearly in anti-phase with one another.

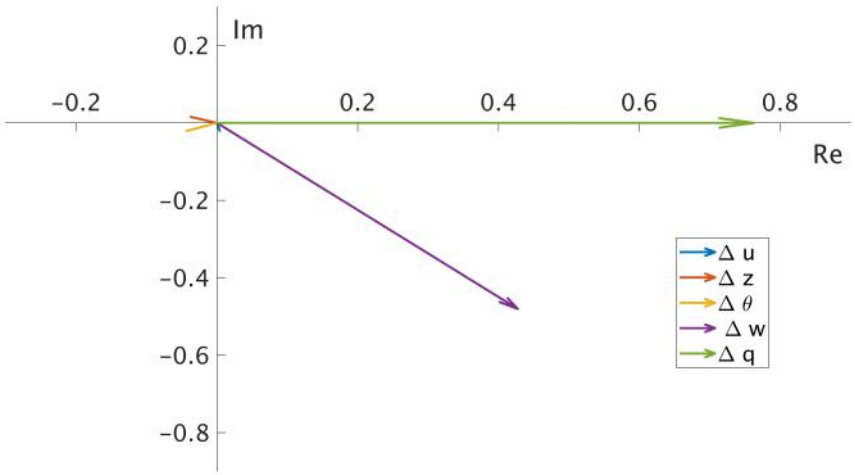

Figure 6.5: A visualisation of the complex eigenvector v_1.

6.3.2 Influence of the Z-board

It is of interest how the different components (primarily the Z-board and elevator) would affect the stability of the boat. In Fig. 6.7 the eigenvalues are shown for three different geometries. For the standard geometry from the previous section, and for the geometries where the individual derivatives of the Z-board are multiplied with 0.5 and 1.5. This corresponds with respectively a certain decrease and increase in surface of the Z-board. It is seen how increasing the derivatives would lead to even more stable modes and also to a shorter period of oscillation. Mainly the complex modes are affected. Notice however that the corresponding increase or decrease in surface, will not always lead to a feasible geometry as static equilibrium is not guaranteed. E.g. it is possible that the foils become to small to generate sufficient force to lift the hull. Needless to say, this variation will also lead to a new equilibrium state.

6.3.3 Influence of the elevator

In Fig. 6.8 the eigenvalues are shown as a function of the individual derivatives of the elevator. As was expected, increasing the elevator derivatives leads to a more stable mode. The effect of the elevator is more pronounced as with the Z-board for a comparable variation. The period of eigenmodes Δx_1 and Δx_2 will also become larger with approximately a factor 3. It is known that the the boat will be unstable if there would be no elevator. This is visualised in Fig.6.9. It can also be noticed how the modes have changed completely: there are now three real eigenvalues and only one complex conjugated pair. This change in modes appear when the derivatives of the elevator are multiplied with 0.103, it is at this moment that eigenmode Δx_5 becomes critically damped. This is shown in Fig. 6.10.

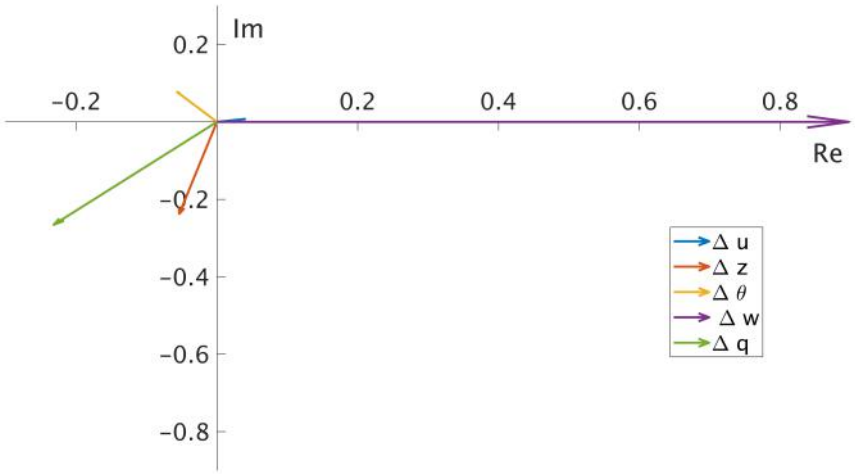

Figure 6.6: A visualisation of the complex eigenvector v_3.

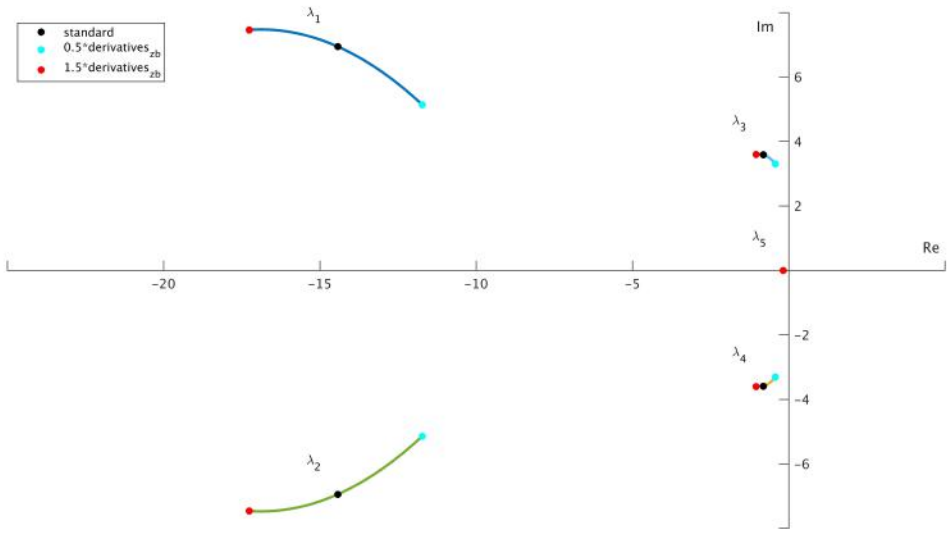

Figure 6.7: A root locus diagram of the eigenvalues as a function of the individual derivatives of the Z-board.

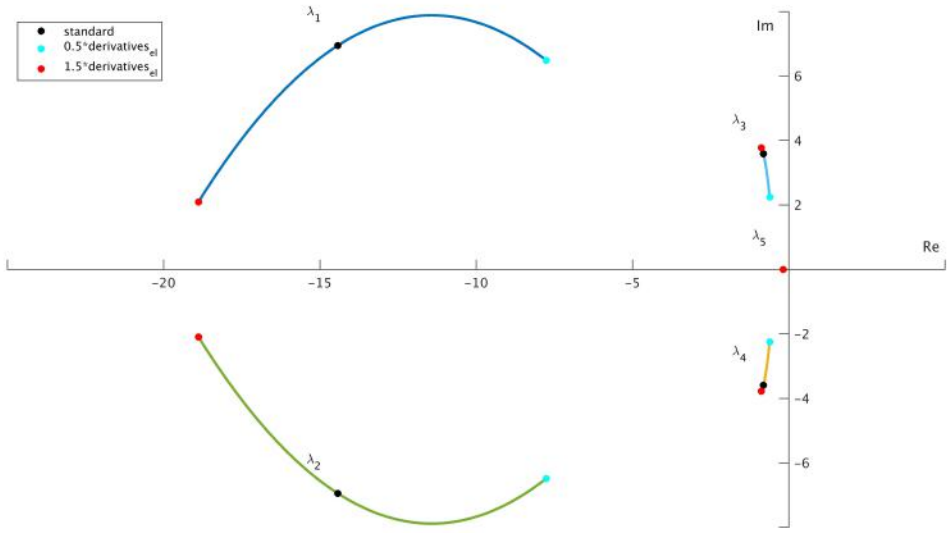

Figure 6.8: A root locus diagram of the eigenvalues as a function of the individual derivatives of the elevator.

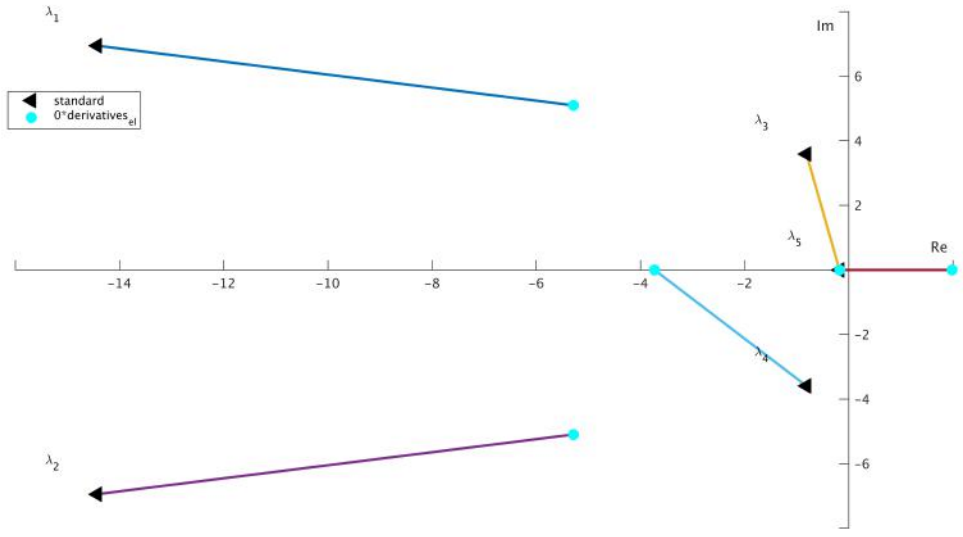

Figure 6.9: A root locus diagram of the eigenvalues for two cases: the standard geometry and a geometry where all the elevator derivatives are zero.

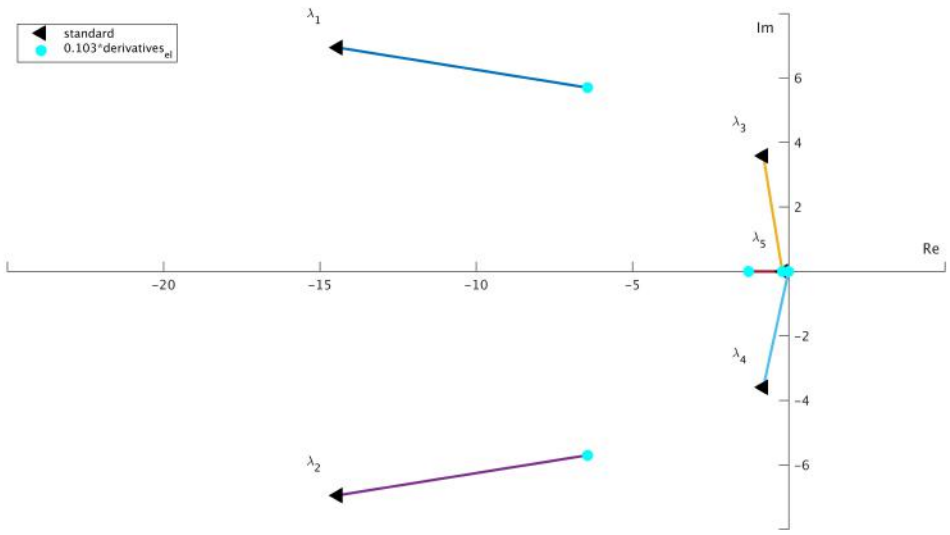

Figure 6.10: A root locus diagram of the eigenvalues for two cases: the standard geometry and a geometry where the boat is critically damped for mode 5.

7 Conclusion

The goal of this thesis was to find a way to quantify the stability of a hydrofoiling boat using CFD. Both Drela's and Masuyama's interpretations on stability dynamics are discussed to have adequate theoretical support on this matter. This thesis can be used as a framework for performing a longitudinal dynamical stability analysis of a hydrofoil boat. In this regard this thesis has managed to fulfil its goal. The idea was also to examine the stability of the Viper more in depth. However, there was only time to look into one state and geometry. There are two distinct parts in the framework: one is the calculation of the equilibrium state and the other is the calculation of the derivatives to examine the stability of this state. This framework contains an approach on how to calculate the equilibrium state of a certain geometry sailing at a certain speed. The algorithm proposed by this approach allows this process to be automated. For the derivatives, approximations were discussed with the purpose of limiting calculation time.

7.1 Results

The longitudinal stability of the Viper's standard geometry was investigated at sailing speed of 10 m/s. 5 longitudinal eigenmodes were found: two complex conjugated pairs of eigenvalues and one real eigenvalue. It could be concluded that the boat was both statically and dynamically stable. The real eigenmode was characterized by a coupled motion between the forward velocity and the draft and trim. This mode was weakly damped. The two complex pairs of eigenmodes gave rise to a motion dominated by heave and pitch. One pair was heavily damped and one was weakly damped. The influence of the derivatives of the individual components was also

examined.

7.2 Future Work

The application of CFD on the dynamic stability analysis of a hydrofoil boat looks promising as hydrofoiling is still a quite new development. However, to make this approach more efficient and more easily applicable, additional research is needed. Both parts comprising the framework, the calculation of the equilibrium state and the construction of the stability matrix, need additional refinement.

A first observation is the lack of experimental data for validation of the calculated equilibrium points and the derivatives. This data could originate from full scale tests or even towing-tank tests with hydrofoils. This will help both aspects of the framework. For example, a really simple geometry for which the equilibrium states are calculated at different speeds. Together with these equilibrium states, the derivatives of the various forces and moments to the various kinematic parameters could be calculated. Such a case could then be used to validate the entire framework.

But also the approaches themselves can be tested and refined. As there was insufficient time, the FSI algorithm was not run with lower convergence thresholds. Consequently it was only used for a 2D case. Running the algorithm for different speeds and different geometries could have proven to help validate this algorithm. Comparing the eigenmodes for the standard geometry at different sailing speeds or comparing them for different geometries at the same speed would also have been mutually beneficent for GD in their development of the foiling Viper and for the further refinement of the algorithm and stability model. Next to the influences of a speed variation, other variations would also lead to interesting results: the influence of the variation of the position of the CoG (crew movement), the influence of the variation of the different rakes of elevator and Z-board, the influence of a different elevator design, ...

A big step forward would be to have a more performant model for the forces and moments generated by the sail. This would not only increase the accuracy of the existing longitudinal model but would also allow to include lateral stability to have a more complete model. In the case at hand the boat has a fixed longitudinal velocity, but if the sail is modelled, this fixed speed could be substituted for a driving force component. This way a variable speed is obtained. The model could then be extended to also make speed predictions as the algorithm for calculating the equilibrium state could be able to balance out the driving force and drag. This would allow to examine the trade-offs between speed and stability. E.g. a certain change in geometry allows for a higher speed in the equilibrium state but is simultaneously detrimental for the stability behaviour.

It can be concluded that this framework can have multiple applications and that are still many areas where it can be improved or extended. The application of CFD for the dynamic stability analysis of a hydrofoil boat proves to have many possibilities.

Bibliography

[1] S. Bayraktar, Y. Ozdemir, and T. Yilmaz, "Computational analysis of wind velocity and direction effects on a sail." 06 2007.

[2] (2016) Photos: Ms amlin international. Last accessed 25 February 2019. [Online]. Available: https://www.sailingscuttlebutt.com/2016/12/09/photos-ms-amlin-international-moth-regatta-2016/

[3] (2013) America's cup 2013. Last accessed 25 February 2019. [Online]. Available: http://www.cupinfo.com/en/americas-cup-2013-oracle-design-andrew-mason-13067.php

[4] M. Altosole, G. Benvenuto, M. Figari, and U. Campora, "Real-time simulation of a cogag naval ship propulsion system," *Proceedings of The Institution of Mechanical Engineers Part M-journal of Engineering for The Maritime Environment*, vol. 223, pp. 47–62, 02 2009.

[5] Y. Masuyama, "Performance of a hydrofoil sailing boat (2 nd report)," *Journal of the Society of Naval Architects of Japan*, no. 152, pp. 202–215, 1982.

[6] ——, "Stability analysis and prediction of performance for a hydrofoil sailing boat," *International Shipbuilding Progress*, vol. 34, no. 390, pp. 20–29, 1987.

[7] R. A. Carter, "Boat remains and maritime trade in the persian gulf during sixth and fifth millennia bc." *Antiquity*, vol. 80, 03 2006.

[8] (2019) History of the americas cup. Last accessed 15 February 2019. [Online]. Available: https://www.americascup.com/en/history

[9] (2010) Viper: Classes and equipment. Last accessed 15 February 2019. [Online]. Available: https://www.sailing.org/classesandequipment/VIP.php

[10] C. A. Marchaj, *Aero-Hydrodynamics of sailing*, 2nd ed. Adlard Coles., 1988.

[11] A. Acosta, "Hydrofoils and hydrofoil craft," *Annual Review of Fluid Mechanics*, vol. 5, no. 1, pp. 161–184, 1973.

[12] M. Drela, *Flight vehicle aerodynamics*. MIT press, 2014.

[13] How is orientation in space represented with euler angles? Last accessed 26 February 2019. [Online]. Available: https://www.mecademic.com/resources/Euler-angles/Euler-angles

[14] Cfd simulation software | ansys fluent. Last accessed 13 May 2019. [Online]. Available: https://www.ansys.com/products/fluids

[15] Overset meshing best practices. Last accessed 20 May 2019. [Online]. Available: https://www.sharcnet.ca/Software/Ansys/17.0/en-us/help/flu_ug/flu_ug_sec_overset_solver_best_practice.html

[16] R. M. A. Lopes, "Calculation of the flow around hydrofoils at moderate reynolds numbers," Ph.D. dissertation, Master's thesis, Instituto Superior Técnico, 2015.

Stability Derivatives

Table 1: Numeric values for the stability derivatives for the case of a 90° wind angle and a 10 m/s boatspeed as provided by Masuyama[6].

	j	st (i=1)	port (i=2)	rear (i=3)	rudder (i=4)	sail (i=5)	total	dimensionless
X_{ji}	u	-1.59	-4.89	-4.23	-1.2	-9.48	-21.39	-0.078
	v	0.2	-4.09	0	0.74	29.08	25.93	0.094
	w	0.23	4.88	-0.57	0	0	4.54	0.017
	p	0.16	-4.96	0	-1.31	55.26	49.15	0.036
	q	-3.21	-12.48	-9.25	-2.11	18.02	-9.03	-0.007
	ϕ	-103.4	131.4	0	0	0	28	0.032
	θ	42.1	48.6	0	-81.7	0	9	0.010
	z	-52	-60	0	-35.2	0	-147.2	-0.268
	$\dot{v}$	0	0	0	0	0	0	0.000
	$\dot{w}$	0	0	0	0	0	0	0.000
	$\dot{p}$	0	0	0	0	0	0	0.000
	$\dot{q}$	0	0	0	0	0	0	0.000

	j	st (i=1)	port (i=2)	rear (i=3)	rudder (i=4)	sail (i=5)	total	dimensionless
L_{ji}	u	-5.5	44	0	-11.2	10.9	38.2	0.139
	v	-22.1	-181.6	0	99.9	-79.9	-183.7	-0.669
	w	-26.4	216.5	0	0	0	190.1	0.692
	p	-18.3	-220.3	0	-176.3	-151.4	-566.3	-0.412
	q	10.9	-98.5	0	-19.8	-20.7	-128.1	-0.093
	ϕ	-518	-2022	0	0	0	-2540	-2.905
	θ	203	-721	0	0	0	-518	-0.592
	z	-250	890	0	0	0	640	1.165
	$\dot{v}$	-0.39	-1.51	0	1.55	0	-0.35	-0.001
	$\dot{w}$	-0.46	1.8	0	0	0	1.34	0.005
	$\dot{p}$	-0.32	-1.83	0	-2.74	0	-4.89	-0.003
	$\dot{q}$	0.37	-1.46	0	0	0	-1.09	-0.001
M_{ji}	u	3.4	26.5	-11.2	-2.1	18	34.6	0.126
	v	26.1	-151.7	0	1.3	-55.3	-179.6	-0.654
	w	31	181	-1198	0	0	-986	-3.590
	p	22	-184	0	-2	-105	-269	-0.196
	q	-19	-100	-2800	-4	-34	-2957	-2.153
	ϕ	300	-936	0	0	0	-636	-0.727
	θ	-113	-325	-155	0	0	-593	-0.678
	z	139	401	-67	0	0	473	0.861
	$\dot{v}$	0.45	-1.2	0	0	0	-0.75	-0.003
	$\dot{w}$	0.54	1.43	-9.64	0	0	-7.67	-0.027
	$\dot{p}$	0.37	-1.46	0	0	0	-1.09	-0.001
	$\dot{q}$	-0.44	-1.16	-22.36	0	0	-23.96	-0.017
Z_{ji}	u	-7.9	-43.2	-1.4	0	0	-52.5	-0.191
	v	-31.8	178.4	0	0	0	146.6	0.534
	w	-37.9	-212.7	-515.9	0	0	-766.5	-2.791
	p	-26.4	216.5	0	0	0	190.1	0.138
	q	16	97	-1199	0	0	-1086	-0.791
	ϕ	-601	1397	0	0	0	796	0.910
	θ	233	490	-67	0	0	656	0.750
	z	-288	-605	-29	0	0	-922	-1.678
	$\dot{v}$	-0.56	1.49	0	0	0	0.93	0.003
	$\dot{w}$	-0.66	-1.77	-4.16	0	0	-6.59	-0.024
	$\dot{p}$	-0.46	1.8	0	0	0	1.34	0.001
	$\dot{q}$	0.54	1.43	-9.64	0	0	-7.67	-0.005
Y_{ji}	u	-6.6	36.3	0	6.4	5.7	41.8	0.152
	v	-26.7	-149.7	0	-56.7	-41.9	-275	-1.001
	w	-31.8	178.4	0	0	0	146.6	0.534
	p	-22.1	-181.6	0	99.9	-79.7	-183.5	-0.134
	q	13.1	-81.2	0	11.2	-10.9	-67.8	-0.049
	ϕ	-505	-1172	0	0	0	-1677	-1.918
	θ	196	-412	0	599	0	383	0.438
	z	-241	508	0	258	0	525	0.956
	$\dot{v}$	-0.46	-1.25	0	-0.88	0	-2.59	-0.009
	$\dot{w}$	-0.56	1.49	0	0	0	0.93	0.003
	$\dot{p}$	-0.39	-1.51	0	1.55	0	-0.35	0.000
	$\dot{q}$	0.45	-1.2	0	0	0	-0.75	-0.001